Rock Physical-Property Measurements for the Nechako Basin Oil and Gas Region, Central British Columbia (Parts of NTS 093B, C, E, F, G, K, L)

A. Kushnir, Centre for Experimental Studies of the Lithosphere, Department of Earth and Ocean Sciences, University of British Columbia, Vancouver, BC V6T 1Z4

G. Andrews, Earth Research Institute, University of California Santa Barbara, Santa Barbara, CA 93106

J.K. Russell, Volcanology and Petrology Laboratory, Department of Earth and Ocean Sciences, University of British Columbia, Vancouver, BC V6T 1Z4

R.J. Enkin, Natural Resources Canada, Geological Survey of Canada–Pacific, 9860 West Saanich Road, Sidney, BC V8L 4B2

L.A. Kennedy, Centre for Experimental Studies of the Lithosphere, Department of Earth and Ocean Sciences, University of British Columbia, Vancouver, BC V6T 1Z4

M.J. Heap, Laboratoire de géophysique expérimentale, Institut de physique du globe de Strasbourg (UMR 7516 CNRS, Université de Strasbourg/EOST), 5 rue René Descartes, 67084 Strasbourg CEDEX, France

S. Quane, Quest University Canada, 3200 University Boulevard, Squamish, BC V8B O8N

Kushnir, A., Andrews, G., Russell, J.K., Enkin, R.J., Kennedy, L.A., Heap, M.J. and Quane, S. (2012): Rock physical-property measurements for the Nechako Basin oil and gas region, central British Columbia (parts of NTS 093B, C, E, F, G, K, L); *in* Geoscience BC Summary of Activities 2011, Geoscience BC, Report 2012-1, p. 125–150.

Abstract

The Mesozoic hydrocarbon-prospective Nechako (sedimentary) Basin in central British Columbia is buried by a variably thick and variably extensive, lithologically diverse assemblage of Cenozoic volcanic and sedimentary rocks. To assist in the interpretation of geophysical surveys, physical and geophysical properties (density, porosity, magnetic susceptibility and remanence, electrical resistivity and chargeability, and seismic velocity) have been measured on a sample suite covering the eleven stratigraphic units within, and stratigraphically above, the Nechako Basin. The eleven basic stratigraphic units are grouped into six major lithostratigraphic packages (combined on the basis of age, geography and lithology) for the purposes of comparing physical and geophysical properties. Each lithostratigraphic package is distinguishable on the basis of one or more physical or geophysical properties; for example, potential Cretaceous reservoir rocks (e.g., Jackass Mountain Group) have relatively high porosities (=17%), low resistivities and low seismic velocities. Generally, volcanic rocks are easily distinguished from sedimentary rocks, and the crystalline basement is distinguished from both. This dataset is available for incorporation into ongoing and future geophysical surveys of the Nechako Basin, and can be used retrospectively to assess previous interpretations. Such integrated datasets are necessary to provide a comprehensive geological and geophysical interpretation.

Keywords: *Nechako Basin, rock properties, physical properties, geophysical properties*

This publication is also available, free of charge, as colour digital files in Adobe Acrobat® PDF format from the Geoscience BC website: http://www.geosciencebc.com/s/DataReleases.asp.

Introduction

The Mesozoic Nechako Basin in south-central British Columbia (BC; Figure 1) has underexplored potential for oil and gas deposits hosted in Cretaceous strata (Hannigan et al., 1994; Hayes, 2002). First-order geological interpretations of the subsurface are hampered by the basin's structural complexity, which results from extensive polyphase deformation and partial burial beneath significant extents and variable thicknesses of Cenozoic volcanic, volcaniclastic and sedimentary rocks (Riddell, 2006, 2011).

The lack of continuity in outcrop and stratigraphy has hindered reconstructions of the basin and efforts to identify potential hydrocarbon traps. In an effort to address this, geophysical surveys were conducted in the mid-2000s across portions of the Interior Plateau (e.g., Kim, 2010; Hayward and Calvert, 2011; Idowu et al., 2011; Spratt and Craven, 2011). Interpretation of these new data, coupled with a reassessment of existing geophysical datasets (e.g., Hayward and Calvert, 2009), is made difficult by a lack of rock physical-property data for the corresponding rocks within the Nechako Basin and a fragmentary understanding of even the near-surface geology (e.g., Dohaney et al., 2010; Andrews et al., 2011). Establishing the extent of buried Cenozoic

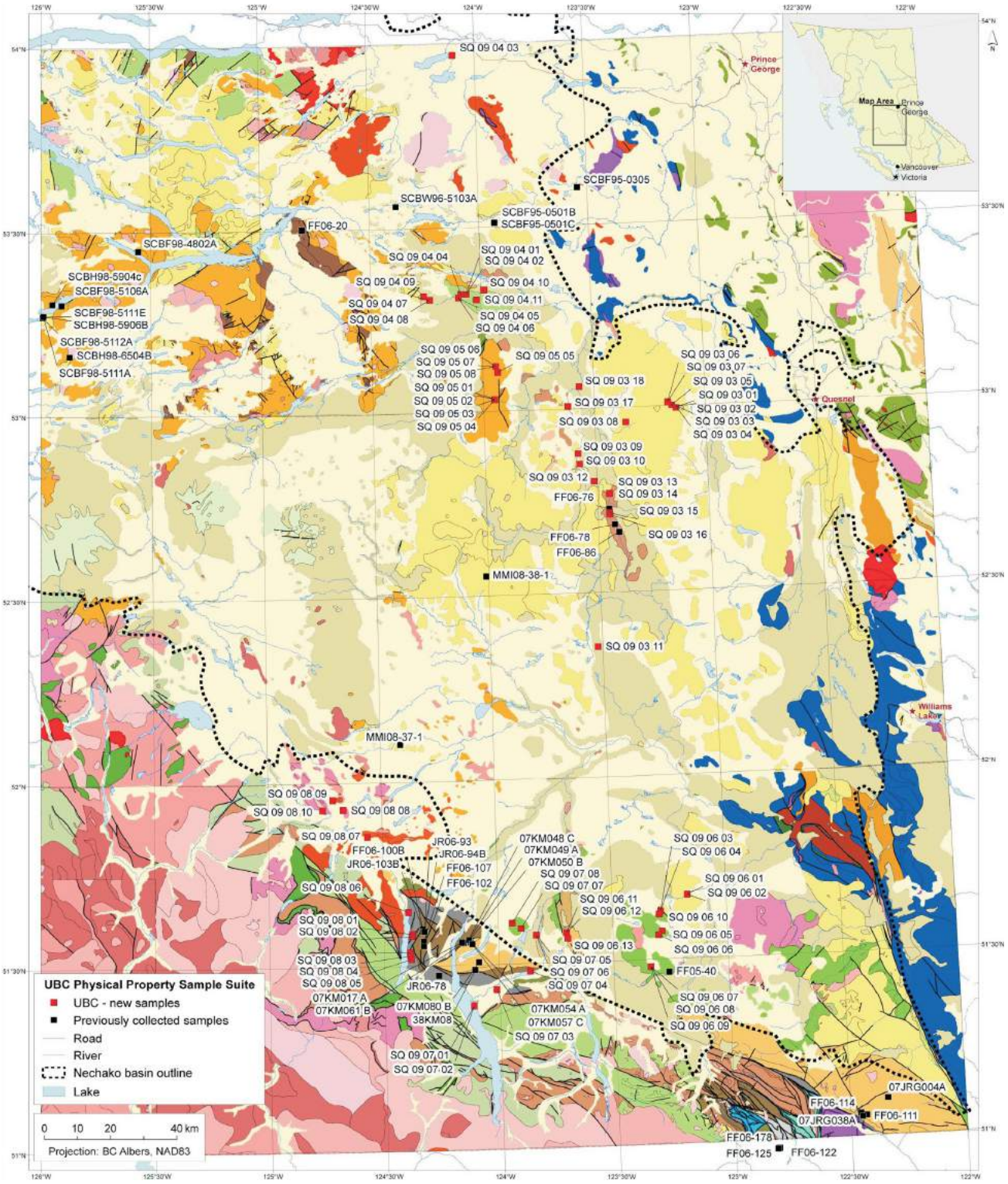

Figure 1. Geology of the Nechako Basin, showing the 81 sample sites and the 167 samples collected. Geology adapted from Riddell (2006) and prepared by F. Ma of Geoscience BC.

volcanic rocks and distinguishing them from buried and deformed Mesozoic successions are particularly challenging.

Geoscience BC funded an investigation of the rock physical properties of the Nechako Basin and overlying units. We assembled a representative suite of 167 samples from existing collections and from a focused field campaign to extend the sample diversity. Samples were prepared at the University of British Columbia and subjected to a comprehensive suite of experiments to measure bulk density, connected porosity, magnetic susceptibility, magnetic remanence, Koenigsberger ratio, electrical resistivity, chargeability and ultrasonic velocity. All measurements were performed at 1) the Centre for Experimental Study of the Lithosphere (CESL) at the University of British Columbia (UBC); 2) the Paleomagnetism and Petrophysics Laboratory at Geological Survey of Canada–Pacific, Sidney (GSC-P); and 3) the Laboratoire de Géophysique Expérimentale at l'Université de Strasbourg, France (EOST). Experimental results are presented as a comprehensive series of tables and crossplots that emphasize parameters that can be used to distinguish between the various units.

This report summarizes the results of the first comprehensive, multiparameter rock-property study of the Nechako Basin and overlying units. The dataset discussed herein is available in Andrews et al. (2011). It is also expected that the associated electronic database will, in turn, be integrated into other provincial and national rock-property databases (e.g., Salisbury and Iuliucci, 2001; Mira Geoscience, 2008; Parsons et al., 2009). These data are intended for use in ongoing and future geophysical experiments, and will enable better differentiation between units;

this will, in turn, allow better understanding of the structure, tectonic evolution and hydrocarbon potential of the Nechako Basin.

Geology of the Nechako Basin

The Nechako Basin is an area of approximately 75 000 km^2 bounded to the south and west by the Coast Mountains, to the north by the Skeena Arch, and to the east by the Bonaparte Plateau and Cariboo Mountains (Figure 1; Hayes, 2002; Riddell, 2006). It underlies much of the present-day Fraser River Basin, including important tributaries such as the Chilcotin, Chilko and Taseko rivers. The Nechako Basin is interpreted to have developed as a foreland basin during the Late Jurassic to mid-Cretaceous on basement comprising integral parts of the Intermontane Superterrane, namely the Cache Creek and Stikine terranes. Stikine terrane basement is present at the surface in the west and north of the basin (Riddell, 2006), where it is represented by the Early–Middle Jurassic Hazelton volcanic arc (Hazelton Group). Oceanic rocks of the Cache Creek terrane rocks outcrop in the east and northeast. There is no inferred hydrocarbon resource in the basement.

The Nechako Basin was filled with clastic sedimentary rocks from the Middle Jurassic (Ladner Group) to the Early Cretaceous (Relay Mountain Group). Clastic marine sedimentation continued through the Cretaceous (Hauterivian–Cenomanian Jackass Mountain Group, Albian Taylor Creek and Skeena groups, and Albian–Cenomanian Silverquick Formation) and was interspersed with deposition of volcanic and volcaniclastic rocks of the Albian–Santonian Spences Bridge and Kasalka groups, and the Turonian–Campanian Powell Creek Formation and informally named Taseko River strata. Numerous Mesozoic and Cenozoic plutons intruded the basin. All appreciable hydrocarbon potential is within the Cretaceous succession. Figure 2 provides a generalized and schematic stratigraphic summary of the basin.

The Nechako Basin is buried beneath 0–4000 m of Eocene, Miocene and Pliocene volcanic, volcaniclastic and sedimentary rocks belonging mainly to the Endako, Ootsa Lake and Chilcotin groups (Riddell, 2006; Andrews and Russell, 2007, 2008; Andrews et al., 2011; Bordet and Hart, 2011). A diverse range of mafic and felsic volcanic and volcaniclastic rocks occur, including ash-flow tuff that is indicative of caldera-forming eruptions. The Pliocene–Holocene Anahim volcanic belt trends east across the centre of the ba-

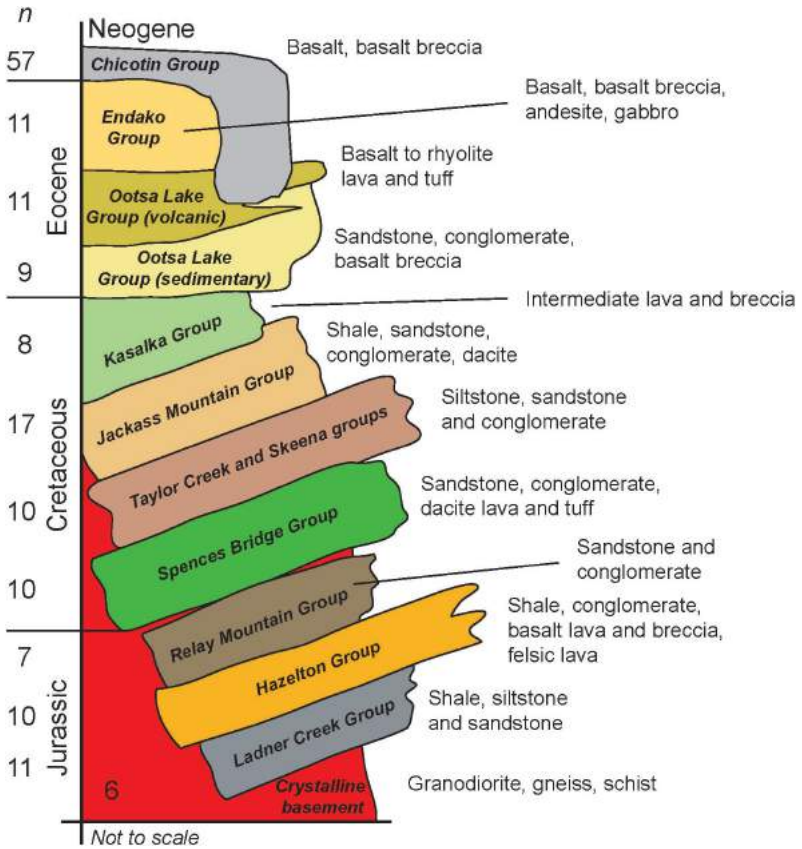

Figure 2. Schematic representation of stratigraphic relationships between map units sampled within the Nechako Basin. Number of samples collected from each stratigraphic unit is given on left.

sin. The basin and overlying Cenozoic rocks are buried beneath a 1–100 m thick veneer of glacial sediments, including till and glaciolacustrine and glaciofluvial successions (e.g., Andrews et al., 2011). There is no inferred hydrocarbon resource in the Cenozoic succession.

The structural geology of the Nechako Basin is poorly understood, so the architecture of potential hydrocarbon traps has not been established. Preliminary geological and geophysical surveys have identified sub-basins (e.g., Hayward and Calvert, 2009), high- and low-angle faults, folds and unconformities (e.g., Mihalynuk et al., 2009); however, a lack of stratigraphic control due to the paucity of boreholes in the basin makes lateral correlation and section-balancing impossible. A dedicated rock-property suite from the known Nechako Basin stratigraphy will allow for improved geophysical imaging of the subsurface geology.

Sample Suite

During the 1980s, seismic-reflection and gravity surveys were completed in the Nechako Basin and additional exploration wells were drilled; new vibroseis seismic-reflection and magnetotelluric datasets were collected in 2008 (Calvert et al., 2009; Craven and Spratt, 2011). There is a pressing need for better constraints on a range of physical and geophysical rock properties from the diverse suite of volcanic and sedimentary rocks in the basin. For example, magnetotelluric studies have highlighted the need for good resolution in electrical-resistivity data to differentiate the widespread Cretaceous and Eocene sequences (e.g., Craven and Spratt, 2011). Similarly, seismic inversions (e.g., Hayward and Calvert, 2009) suggest nonintuitive variations in compressional-wave velocities for individual formations, specifically overlap in inferred seismic velocities between the Eocene and Jurassic–Cretaceous successions. Quantitative, experimental physical-properties data from this sample suite will aid the interpretations of these surveys and help to distinguish the prospective, non-hydrocarbon Eocene basinal sequence from the Jurassic–Cretaceous basinal sequence.

The UBC experimental program identified and sampled stratigraphic groups that are most important to the interpretation of seismic datasets and the delineation of exploration targets within the Nechako Basin (Figure 2, Table 1).

The **Chilcotin Group** (CB, Table 1) comprises Miocene-age basaltic lavas. The Chilcotin is areally extensive and comprises thin (<50 m) basaltic lavas and breccias. The porosity (vesicularity) of these deposits is highly variable laterally and with depth. Infilled paleovalley sections may be up to 200 m thick and filled mainly with porous, poorly consolidated breccias (Andrews and Russell, 2007).

The package of **Eocene volcanic and sedimentary rocks** (EVS, Table 1) features deposits that are highly variable in thickness (absent to >1000 m) and, in part, cover the Jurassic and Cretaceous rocks that form the Nechako Basin. These stratigraphic units blanket, obscure and complicate the interpretation of structure and stratigraphy of the Jurassic source rocks and Cretaceous reservoir rocks. Specific lithostratigraphic packages studied include the Endako and Ootsa Lake groups (e.g., Bordet and Hart, 2011). The Endako Group comprises coherent, mafic lavas, which need to be distinguished from Chilcotin Group rocks. The Ootsa Lake Group includes both volcaniclastic and coherent facies. The volcaniclastic succession comprises a series

Table 1. Description of sample suite in terms of stratigraphic group and lithological type.

Group name	No. of samples (N)	Lithological types	Stratigraphic package
Chilcotin	57	Vesicular basaltic lava; basaltic breccia	CB
Endako	11	Vesicular basaltic lava; amygdaloidal basalt lava; basalt breccia; andesite; gabbro	EVS
Ootsa Lake (coherent)	11	Intermediate and felsic lava; rhyolitic welded tuff; basaltic lava; microgranite	EVS
Ootsa Lake (noncoherent)	9	Sandstone; conglomerate; volcanic breccia	EVS
Kasalka / Powell Creek / Taseko River	8	Andesite; lapilli tuff; breccia; conglomerate	KVS
Jackass Mountain	17	Arkose conglomerate; black shale; dacite intrusions; sandstone	KVS
Taylor Creek and Skeena	10	Sandstone; chert-pebble conglomerate; siltstone	KVS
Spences Bridge	10	Dacite lava; conglomerate; sandstone; andesitic tuff	KVS
Relay Mountain	7	Sandstone; conglomerate	JS
Ladner	11	Calcareous shale; shale; sandstone	JS
Hazelton	10	Felsic lava; volcanic breccia; mudstone; sandstone; granite; conglomerate; shale	JVS
Mesozoic Plutonic	6	Granodiorite, diorite, orthogneiss	MB_P

of felsic volcaniclastic rocks and associated bedded sedimentary rocks, and are difficult to discriminate geophysically from older Cretaceous volcaniclastic and sedimentary successions. Coherent facies are defined by intermediate to felsic lavas and lava domes, which need to be discriminated from Endako Group lavas.

The **Cretaceous volcaniclastic and sedimentary rocks** (KVS, Table 1) are the potential hydrocarbon reservoir rocks within the Nechako Basin. They are strongly bedded, weakly deformed and of exceptionally variable thickness. The lateral continuity of stratigraphy has not yet been fully resolved (Ferri and Riddell, 2006), so it was necessary to sample several units in multiple locations. Despite this procedure, we acknowledge that there may be facies variations of these units that remain unsampled. We have characterized the geophysical properties of the following lithostratigraphic packages within this broad time grouping:

- Jackass Mountain Group: coarse-grained clastic sedimentary rocks inferred to be the most likely surface correlative of the subsurface Skeena assemblage, which has been identified as the most significant potential reservoir in the Nechako Basin (MacLaurin et al., 2011); best exposed and studied along the southern margin of the Nechako Basin near Taseko Lake

- Taylor Creek Group and Skeena Group: clastic sedimentary rocks and minor volcanic rocks exposed along, and encountered in the subsurface of, the Nazko River area

- Spences Bridge Group: intermediate lavas and tuffs, and minor sedimentary rocks exposed in the southern Nechako Basin

- Kasalka Group, Powell Creek Group and 'Taseko River strata': intermediate lavas and tuffs, and associated clastic sedimentary rocks (including conglomerate and sandstone in the 'Taseko River strata') found in many areas throughout the basin; likely a very extensive sequence

The **Middle–Late Jurassic sedimentary rocks** (JS, Table 1) are the most probable source rocks for hydrocarbon reserves hosted by the Nechako Basin. This lithostratigraphic package is expected to form the lowermost parts of the basinal sequence. Our sampling includes 1) the Ladner Group, comprising fine- to coarse-grained calcareous clastic rocks and carbonates exposed around Chilko Lake in the southern part of the basin; and 2) the Relay Mountain Group, best exposed in the Nemaiah Valley and Chilko Lake areas in the southern part of the basin and comprising fine- to coarse-grained clastic and carbonaceous rocks that underlie the Jackass Mountain Group.

The **Lower–Middle Jurassic volcanic and sedimentary rocks** (JVS, Table 1) are a package of intermediate to felsic lavas and tuffs, and minor clastic and carbonate sedimentary rocks (e.g., Puntzi Lake and west of Nechako).

The last package of samples is the **Mesozoic basement rocks** (MB_p, Table 1). The Nechako Basin is underlain by Permian, Triassic and Jurassic rocks of the Cache Creek and Stikine terranes, and intrusions of Jurassic–Eocene age. These rocks tend to be more homogeneous in character and more easily differentiated from the overlying Cretaceous and Eocene stratigraphy. The more abundant of these stratigraphic units include 1) Jurassic–Cretaceous intrusive rocks (e.g., Taseko River); and 2) the mid-Triassic Cache Creek Group, comprising limestone, chert, clastic sediments, metamorphic rocks and basalt (e.g., Blackwater River, Hanceville).

Methodology

A large suite of rock samples was collected from formations representing the key Mesozoic and Tertiary rock types/stratigraphic units within the Nechako Basin. From this collection, 167 samples were chosen for experimental work to be performed at CESL (UBC), GSC-P and EOST. The Nechako sample suite comprises rocks of various types, sampled from 12 distinct stratigraphic units distributed across the Nechako Basin. Each of the 167 samples was drilled to obtain a cylindrical rock core measuring 25 mm in diameter by ~50 mm in length. The ends of each core were ground and polished at right angles to the cylinder side to create a smooth (~0.02 mm precision) end surface. The polished ends are critical for the experimental measurement of seismic velocity because they provide perfect sample geometry and ensure that there is good contact between the end caps of the seismic-velocity transducer and the sample. All sample preparation (e.g., cleaning, trimming, coring, drying) was carried out at CESL, with some modification at EOST. Different sets of geophysical properties were measured on the same sample cores by JKR's team at CESL and EOST, and by RJE's team at GSC-P. The following properties were measured for each sample core: bulk density (EOST), porosity (EOST), magnetic susceptibility (CESL and GSC-P), remanent magnetization (GSC-P), electrical resistivity (GSC-P), induced-polarization chargeability (GSC-P), and seismic-wave velocities (EOST and CESL). These data are given in Tables 2 and 3.

Density and Porosity

Dry bulk density (ρ_d), wet bulk density (ρ_w) and framework density (ρ_f) were measured for all samples. Bulk density is the density of the entire sample (i.e., rock plus pore space). The pore space includes connected and isolated pores. Bulk densities are calculated from the geometry and mass (dry or wet) of the sample core. The framework density is the den-

sity of the rock itself (i.e., excluding pore space) and is measured using the hydrostatic weighing method, as derived from Archimedes' Buoyancy Law. Using this method, the framework density actually measures the density of the rock and its isolated porosity, if there is any present. In the Nechako Basin sample suite, isolated porosity is assumed to be negligible.

All sample cores were dried at 40°C under a vacuum for 24 hours. After the dry mass (m_d) of each core was measured, all samples were vacuum saturated with agitated, deionized, distilled water for a minimum of 15 hours to allow the water to fill all connected pore space within the sample. The mass of the water-saturated sample was then weighed in air (m_w) and while it was fully submerged in water (m_b). Wet bulk density (ρ_w) was calculated for each water-saturated sample to estimate the density of the rock plus its water-saturated pore space and any residual isolated pore space. These values are required for determination of wet seismic velocity.

The density of the rock framework (plus any remaining isolated pores) was then computed using the relationship

$$\rho_f = \rho_{H_2O} \frac{m_d}{m_d + m_b}, \quad (1)$$

where (ρ_{H2O}) is the density of the water under ambient lab conditions. Values of ρ_d and ρ_f are sufficient to estimate porosity (%) using

$$\phi = 100 \times \frac{m_w - m_d}{m_w - m_b}. \quad (2)$$

Magnetic Susceptibility

Magnetic susceptibility (k) is primarily a result of the presence of magnetic minerals in rocks, magnetite being the most ubiquitous of these minerals (Telford et al., 1976). There is substantial variability in k within and between rock types (Telford et al., 1976). For instance, igneous rocks have the highest average k values (0–200 × 10^3 SI), whereas metamorphic rocks range between 0 and 70 × 10^3 SI, and sedimentary rocks between 0 and 20 × 10^3 SI (Telford et al., 1976).

Magnetic susceptibility was measured on hand samples in the lab using a GF Instruments model SM-20 pocket magnetic-susceptibility meter, with a sensitivity of 10^{-6} SI volume units. The measurement coil has a 5 cm diameter, and ~90% of the measured response comes from the top 2 cm of the sample. We investigated the effect of small sample size on the measurements and found that samples more than 3 cm thick allow accurate magnetic-susceptibility determinations. Generally, three measurements were taken on different surfaces of the sample and the average is reported. The standard deviation of the three measurements is typically 10% due to spatial variations in magnetite concentration. Susceptibility measurements on cores were measured with a Sapphire Instruments model SI2B susceptibility meter, accurate to 10^{-7} SI. These measurements were used in preference to the SM-20 measurements.

Magnetic Remanence and Koenigsberger Ratio

Natural remanent magnetization (NRM), if present, is a significant contributor to the overall magnetization of rocks (Telford et al., 1976). Magnetization is strongly dependent on the existing magnetic field and the mineralogical content of rocks, as well as the impact of emplacement conditions (Telford et al., 1976). Most relevant to the Nechako Basin is thermoremanent NRM due to the emplacement of hot volcanic rocks.

Magnetic remanence was measured using an Agico Inc. model JR5-A spinner magnetometer (sensitivity 10^{-5} A/m). The full vector was measured, but only the total vector magnitude of the remanence is reported in the database. The Koenigsberger ratio (K_N) compares the relative strength of the natural remanent magnetization (NRM) to the induced magnetism in the geomagnetic field and is calculated as

$$K_N = NRM / (H_0 \chi 0), \quad (3)$$

where $\chi 0$ is the magnetic susceptibility and the geomagnetic field strength (H_0) is approximated as a constant 40 A/m (or $\mu_0 H_0$ = 50 μT = 50000 γ). For K_N >1, magnetic-anomaly interpretation will be incorrect if magnetic remanence is not taken into consideration.

Electrical Resistivity and Chargeability

Complex electrical-impedance frequency spectra were measured using a Solartron Analytical model 1260 impedance spectrum analyzer, based on the method of Katsube (2001). Sample cylinders were vacuum impregnated in distilled water and allowed to soak for at least 24 hours, to allow original groundwater solutes precipitated in the sample porosity to dissolve and approximate original groundwater conductivity. The impedance was measured with five frequencies per decade from 1 MHz to 0.03 Hz. The scalar resistance was picked as the real impedance at the frequency that displays minimum imaginary impedance, typically around 1000 Hz. Resistivity (in ohm·m, or Ω·m) is the scalar resistance multiplied by the sample geometric factor (i.e., the cross-sectional area divided by the length). Conductivity (Mho/m) is the reciprocal of the resistivity.

Induced-polarization chargeability was calculated after converting the frequency-domain impedance spectrum to the time-domain response to a step function, $V(t)$. Using the Newmont Standard (Sumner, 1976), the chargeability (m_T) is

$$m_T = \int_{400ms}^{1100ms} \frac{V(t)}{V(0)} dt. \quad (4)$$

Table 2. Physical and geophysical properties of Nechako Basin sample suite, organized by stratigraphic groups (Table 1) and summarized as maximum, minimum and average values.

	Group name:	Chilcotin[1,2]	Endako	Ootsa Lake (coherent)	Ootsa Lake (noncoherent)	Kasalka / Powell Creek / Taseko River	Jackass Mountain
Dry average V_P (km/s)[3]	Max.	5.99	5.82	5.72	5.19	5.66	6.17
	Min.	4.24	3.31	3.25	2.25	4.23	3.25
	Avg.	5.25	4.93	4.40	3.44	4.73	5.24
Wet average V_P (km/s)[3]	Max.	n/a	6.63	5.81	5.52	5.91	6.49
	Min.	n/a	3.88	4.16	3.62	4.78	4.82
	Avg.	n/a	5.53	4.98	4.40	5.36	5.82
Dry average V_S (km/s)[3]	Max.	n/a	3.44	3.25	2.43	2.96	3.33
	Min.	n/a	1.59	2.08	1.04	1.97	1.99
	Avg.	n/a	2.64	2.60	1.49	2.56	2.79
Wet average V_S (km/s)[3]	Max.	n/a	4.10	3.40	2.67	3.07	3.65
	Min.	n/a	1.77	1.77	1.50	2.15	1.67
	Avg.	n/a	2.81	2.54	1.98	2.67	2.83
Dry bulk density (g/cc)[3]	Max.	2.99	2.89	2.68	2.65	2.87	2.80
	Min.	2.49	1.98	2.23	1.87	2.41	2.54
	Avg.	2.72	2.53	2.43	2.13	2.64	2.70
Wet bulk density (g/cc)[3]	Max.	n/a	2.90	2.69	2.67	2.89	2.80
	Min.	n/a	2.25	2.35	2.16	2.49	2.60
	Avg.	n/a	2.61	2.49	2.31	2.69	2.72
Wet framework density (g/cc)[3]	Max.	3.02	3.02	2.75	2.75	2.91	2.82
	Min.	2.56	2.47	2.45	2.47	2.64	2.67
	Avg.	2.87	2.78	2.59	2.66	2.78	2.75
Dry Poisson's ratio	Max.	n/a	0.36	0.29	0.41	0.40	0.38
	Min.	n/a	0.22	0.08	0.36	0.12	0.20
	Avg.	n/a	0.30	0.22	0.38	0.27	0.29
Wet Poisson's ratio	Max.	n/a	0.45	0.39	0.45	0.38	0.45
	Min.	n/a	0.04	0.23	0.18	0.26	0.23
	Avg.	n/a	0.30	0.32	0.35	0.33	0.33
Dry Young's modulus (GPa)	Max.	n/a	84.36	64.82	42.45	52.01	78.45
	Min.	n/a	13.44	22.67	5.49	28.62	24.18
	Avg.	n/a	48.54	41.53	15.29	43.94	56.62
Wet Young's modulus (GPa)	Max.	n/a	94.08	69.94	51.17	71.57	93.62
	Min.	n/a	19.31	20.83	13.87	31.63	21.23
	Avg.	n/a	55.45	43.68	25.82	52.12	59.94
Dry V_P/V_S	Max.	n/a	2.13	1.83	2.53	2.43	2.24
	Min.	n/a	1.67	1.48	2.14	1.52	1.63
	Avg.	n/a	1.89	1.69	2.32	1.88	1.89
Wet V_P/V_S	Max.	n/a	3.20	2.40	3.30	2.27	3.28
	Min.	n/a	1.44	1.68	1.60	1.75	1.68
	Avg.	n/a	2.07	2.00	2.31	2.03	2.15
Porosity (%)[3]	Max.	16.55	26.74	14.06	29.44	8.42	6.06
	Min.	0.15	0.75	0.32	1.60	1.18	0.27
	Avg.	5.57	8.25	5.68	18.76	4.63	1.72
Magnetic susceptibility (SI)[1,2]	Max.	0.11	0.05	0.04	0.03	0.04	0.01
	Min.	b.d.	b.d.	0.01	b.d.	b.d.	b.d.
	Avg.	0.01	0.01	0.01	0.01	0.01	b.d.
Resistivity (ohm-m)[1]	Max.	95646	17560	23035	9941	20796	29011
	Min.	127	49	82	37	139	116
	Avg.	4541	6135	5098	1518	4886	5101
Koenigsberger ratio (K_N)[1]	Max.	80.90	34.90	6.95	23.35	25.28	30.38
	Min.	0.09	0.01	0.09	0.04	0.06	0.08
	Avg.	13.03	10.24	2.28	8.23	5.37	3.77
Natural remanent magnetization (NRM; A/m)[1]	Max.	48.00	24.80	2.66	27.70	11.70	15.10
	Min.	b.d.	b.d.	0.04	b.d.	b.d.	b.d.
	Avg.	3.17	3.47	0.78	5.37	3.06	1.04
Chargeability (ms)[3]	Max.	n/a	18.70	15.10	11.90	45.20	19.10
	Min.	n/a	0.01	0.03	0.02	0.36	0.28
	Avg.	n/a	5.76	3.36	3.85	7.89	4.48

[1]Measurements conducted at Centre for Experimental Study of the Lithosphere at University of British Columbia (CESL-UBC) under supervision of J.K. Russell.

[2]Measurements conducted at Geological Survey of Canada Pacific, Sidney (GSC-P) under supervision of R.J. Enkin.

[3]Measurements conducted at Laboratoire de G ophysique Exp rimentale at l Universit de Strasbourg, France (EOST) under supervision of M.J. Heap. All seismic velocity measurements (except Chilcotin basalt samples) made under atmospheric pressure with nominal stress of 1 MPa applied to ends of sample. Compressional wave (P-wave) measurements made on samples using a frequency of 700 kHz; shear wave (S-wave) measurements made using a frequency of 300 kHz.

Abbreviations: b.d., below detection; n/a, not measured; VP, P-wave velocity; VS, S-wave velocity.

Table 2 (continued)

	Group name:	Taylor Creek and Skeena	Spences Bridge	Relay Mountain	Ladner	Hazelton	Mesozoic plutonic
Dry average V_P (km/s)[3]	Max.	4.79	5.81	5.61	5.85	5.96	5.46
	Min.	1.65	3.42	4.20	5.22	2.57	3.44
	Avg.	3.40	5.12	5.17	5.65	4.33	4.31
Wet average V_P (km/s)[3]	Max.	5.27	6.15	5.78	6.21	6.50	6.07
	Min.	3.02	4.39	5.16	5.47	3.40	4.33
	Avg.	4.16	5.57	5.60	5.86	5.21	5.45
Dry average V_S (km/s)[3]	Max.	3.22	3.47	3.11	3.39	4.04	3.15
	Min.	1.04	1.89	2.45	3.20	1.51	2.00
	Avg.	2.16	2.84	2.88	3.32	2.39	2.61
Wet average V_S (km/s)[3]	Max.	3.11	3.56	3.52	3.39	3.66	3.33
	Min.	1.47	1.99	2.07	3.03	1.66	2.18
	Avg.	2.28	2.80	2.83	3.24	2.59	2.73
Dry bulk density (g/cc)[3]	Max.	2.63	2.87	2.80	2.77	2.75	2.78
	Min.	2.05	2.30	2.51	2.19	1.91	2.33
	Avg.	2.34	2.63	2.68	2.60	2.45	2.65
Wet bulk density (g/cc)[3]	Max.	2.65	2.87	2.81	2.77	2.76	2.79
	Min.	2.21	2.45	2.54	2.20	2.21	2.45
	Avg.	2.45	2.68	2.70	2.61	2.54	2.68
Wet framework density (g/cc)[3]	Max.	2.73	2.99	2.82	2.80	2.78	2.82
	Min.	2.65	2.66	2.72	2.74	2.62	2.65
	Avg.	2.68	2.81	2.77	2.76	2.71	2.74
Dry Poisson's ratio	Max.	0.29	0.35	0.35	0.27	0.37	0.25
	Min.	0.09	0.20	0.20	0.14	0.07	0.14
	Avg.	0.15	0.27	0.26	0.23	0.24	0.21
Wet Poisson's ratio	Max.	0.42	0.44	0.42	0.30	0.42	0.37
	Min.	0.03	0.17	0.18	0.25	0.06	0.28
	Avg.	0.23	0.31	0.31	0.28	0.32	0.33
Dry Young's modulus (GPa)	Max.	54.42	78.59	66.15	76.53	96.54	69.20
	Min.	5.21	23.85	37.49	62.64	11.52	26.32
	Avg.	28.66	55.50	56.99	70.23	38.38	45.42
Wet Young's modulus (GPa)	Max.	57.48	85.20	78.46	81.94	78.79	79.58
	Min.	15.24	30.47	33.12	51.70	17.62	31.00
	Avg.	32.90	55.93	57.82	70.50	47.53	54.60
Dry V_P/V_S	Max.	1.85	2.08	2.06	1.78	2.21	1.73
	Min.	1.49	1.63	1.63	1.54	1.33	1.55
	Avg.	1.58	1.81	1.80	1.71	1.84	1.66
Wet V_P/V_S	Max.	2.76	3.02	2.76	1.86	2.64	2.20
	Min.	1.43	1.59	1.60	1.74	1.46	1.82
	Avg.	1.90	2.05	2.05	1.81	2.07	2.01
Porosity (%)[3]	Max.	17.07	16.21	3.49	1.60	30.06	11.97
	Min.	2.54	0.60	0.35	0.19	0.43	1.00
	Avg.	11.37	5.11	1.87	0.81	8.48	3.41
Magnetic susceptibility (SI)[1,2]	Max.	b.d.	0.01	b.d.	b.d.	0.04	0.01
	Min.	b.d.	b.d.	b.d.	b.d.	b.d.	b.d.
	Avg.	b.d.	b.d.	b.d.	b.d.	0.01	0.01
Resistivity (ohm-m)[1]	Max.	3650	3433	19199	49883	12338	10771
	Min.	208	428	460	1586	46	152
	Avg.	1190	1635	5348	8617	3864	4402
Koenigsberger ratio (K_N)[1]	Max.	1.37	23.43	0.16	24.90	45.35	5.90
	Min.	0.13	0.68	0.04	0.02	0.05	0.69
	Avg.	0.66	9.19	0.09	2.56	7.78	3.64
Natural remanent magnetization (NRM; A/m)[1]	Max.	0.02	4.77	0.02	1.03	4.56	2.52
	Min.	b.d.	0.14	b.d.	b.d.	b.d.	0.03
	Avg.	b.d.	1.21	b.d.	0.10	1.38	0.98
Chargeability (ms)[3]	Max.	19.60	11.80	5.46	55.60	16.80	23.40
	Min.	0.07	1.15	0.30	0.47	0.89	3.30
	Avg.	4.62	5.59	1.73	7.22	4.85	14.73

Table 3. Physical and geophysical properties of Nechako Basin sample suite, organized by packages on the basis of lithostratigraphy and summarized as maximum, minimum and average values.

Package name:		Miocene Chilcotin (CB)	Eocene Volcanic and Sedimentary (EVS)	Cretaceous Volcanic and Sedimentary (KVS)
Group name:			Endako, Ootsa Lake	Kasalka / Powell Creek / Taseko River, Jackass Mountain, Taylor Creek and Skeena, Spences Bridge
No of samples:		57	31	45
Dry average V_P (km/s)	Max.	5.99	5.82	6.17
	Min.	4.24	2.25	1.65
	Avg.	5.25	4.40	4.67
Wet average V_P (km/s)	Max.	n/a	6.63	6.49
	Min.	n/a	3.62	3.02
	Avg.	n/a	5.08	5.27
Dry average V_S (km/s)	Max.	n/a	3.44	3.47
	Min.	n/a	1.04	1.04
	Avg.	n/a	2.37	2.61
Wet average V_S (km/s)	Max.	n/a	4.10	3.65
	Min.	n/a	1.50	1.47
	Avg.	n/a	2.52	2.66
Dry bulk density (g/cc)	Max.	2.99	2.89	2.87
	Min.	2.49	1.87	2.05
	Avg.	2.72	2.41	2.59
Wet bulk density (g/cc)	Max.	n/a	2.90	2.89
	Min.	n/a	2.16	2.21
	Avg.	n/a	2.50	2.64
Wet framework density (g/cc)	Max.	3.02	3.02	2.99
	Min.	2.56	2.45	2.64
	Avg.	2.87	2.69	2.76
Dry Poisson's ratio	Max.	n/a	0.41	0.40
	Min.	n/a	0.08	0.09
	Avg.	n/a	0.29	0.25
Wet Poisson's ratio	Max.	n/a	0.45	0.45
	Min.	n/a	0.04	0.03
	Avg.	n/a	0.32	0.30
Dry Young's modulus (GPa)	Max.	n/a	84.36	78.59
	Min.	n/a	5.49	5.21
	Avg.	n/a	38.56	47.22
Wet Young's modulus (GPa)	Max.	n/a	94.08	93.62
	Min.	n/a	13.87	15.24
	Avg.	n/a	44.51	50.86
Dry V_P/V_S	Max.	n/a	2.53	2.43
	Min.	n/a	1.48	1.49
	Avg.	n/a	1.91	1.79
Wet V_P/V_S	Max.	n/a	3.30	3.28
	Min.	n/a	1.44	1.43
	Avg.	n/a	2.10	2.04
Porosity (%)	Max.	16.55	29.44	17.07
	Min.	0.15	0.32	0.27
	Avg.	5.57	9.64	5.57
Magnetic susceptibility (SI)	Max.	0.11	0.05	0.04
	Min.	b.d.	b.d.	b.d.
	Avg.	0.01	0.01	b.d.
Resistivity (ohm-m)	Max.	95646	23035	29011
	Min.	127	37	116
	Avg.	4541	4445	3521
Koenigsberger ratio (K_N)	Max.	80.9	34.9	30.4
	Min.	0.1	b.d.	0.1
	Avg.	13.0	6.8	4.1
Natural remanent magnetization (NRM; A/m)	Max.	48.0	27.7	15.1
	Min.	b.d.	b.d.	b.d.
	Avg.	3.17	3.05	1.22
Chargeability (ms)	Max.	n/a	18.7	45.2
	Min.	n/a	0.0	0.1
	Avg.	n/a	4.4	5.4

Abbreviations: b.d., below detection; n/a, not measured

Table 3 (continued)

Package name:		Middle Late Jurassic Sedimentary (JS)	Lower Middle Jurassic Volcanic and Sedimentary (JVS)	Mesozoic Basement (MB_p)
Group name:		**Relay Mountain, Ladner**	**Hazelton**	
No of samples:		**18**	**10**	**6**
Dry average V_P (km/s)	Max.	5.85	5.96	5.46
	Min.	4.20	2.57	3.44
	Avg.	5.38	4.33	4.31
Wet average V_P (km/s)	Max.	6.21	6.50	6.07
	Min.	5.16	3.40	4.33
	Avg.	5.72	5.21	5.45
Dry average V_S (km/s)	Max.	3.39	4.04	3.15
	Min.	2.45	1.51	2.00
	Avg.	3.08	2.39	2.61
Wet average V_S (km/s)	Max.	3.52	3.66	3.33
	Min.	2.07	1.66	2.18
	Avg.	3.01	2.59	2.73
Dry bulk density (g/cc)	Max.	2.80	2.75	2.78
	Min.	2.19	1.91	2.33
	Avg.	2.65	2.45	2.65
Wet bulk density (g/cc)	Max.	2.81	2.76	2.79
	Min.	2.20	2.21	2.45
	Avg.	2.66	2.54	2.68
Wet framework density (g/cc)	Max.	2.82	2.78	2.82
	Min.	2.72	2.62	2.65
	Avg.	2.76	2.71	2.74
Dry Poisson's ratio	Max.	0.35	0.37	0.25
	Min.	0.14	0.07	0.14
	Avg.	0.25	0.24	0.21
Wet Poisson's ratio	Max.	0.42	0.42	0.37
	Min.	0.18	0.06	0.28
	Avg.	0.30	0.32	0.33
Dry Young's modulus (GPa)	Max.	76.53	96.54	69.20
	Min.	37.49	11.52	26.32
	Avg.	62.88	38.38	45.42
Wet Young's modulus (GPa)	Max.	81.94	78.79	79.58
	Min.	33.12	17.62	31.00
	Avg.	63.46	47.53	54.60
Dry V_P/V_S	Max.	2.06	2.21	1.73
	Min.	1.54	1.33	1.55
	Avg.	1.76	1.84	1.66
Wet V_P/V_S	Max.	2.76	2.64	2.20
	Min.	1.60	1.46	1.82
	Avg.	1.94	2.07	2.01
Porosity (%)	Max.	3.49	30.06	11.97
	Min.	0.19	0.43	1.00
	Avg.	1.40	8.48	3.41
Magnetic susceptibility (SI)	Max.	b.d.	0.04	0.01
	Min.	b.d.	b.d.	b.d.
	Avg.	b.d.	0.01	0.01
Resistivity (ohm-m)	Max.	49883	12338	10771
	Min.	460	46	152
	Avg.	7271	3864	4402
Koenigsberger ratio (K_N)	Max.	24.9	45.4	5.9
	Min.	b.d.	0.1	0.7
	Avg.	1.5	7.8	3.6
Natural remanent magnetization (NRM; A/m)	Max.	1.0	4.6	2.5
	Min.	b.d.	b.d.	b.d.
	Avg.	0.06	1.38	0.98
Chargeability (ms)	Max.	55.6	16.8	23.4
	Min.	0.3	0.9	3.3
	Avg.	5.0	4.9	14.7

The main parameters affecting chargeability in laboratory experiments are mineralogy, grain size and the presence of pore-filling ionic fluids (Telford et al., 1976). Chargeability is increased by large surface-to-volume ratios between grains (Telford et al., 1976). Values of chargeability for common rock types vary over 3–4 orders of magnitude: 10–20 ms for carbonate rocks versus 2000–3000 ms for sulphide minerals (Telford et al., 1976). Of particular interest to the Nechako Basin dataset are the average ranges of chargeability cited for volcanic tuff (300–800 ms), dense volcanic rocks (100–500 ms), sedimentary rocks (100–500 ms) and igneous rocks (10–50 ms; Telford et al., 1976).

Seismic Wave Velocities

Two fundamental body-wave types travel through material: compressional (P) waves and shear (S) waves. For P waves, material moves parallel to the direction of propagation; for S waves, material moves in a plane perpendicular to the direction of wave propagation. For energy to travel through a given elastic material, there must be a resulting restoring force that resists deformation (Telford et al., 1976). For instance, when a material experiences strain, that strain must be accommodated by a change in shape of the material. Because fluids cannot sustain a shear force, S waves do not propagate through fluids. The P-wave arrivals are always precursory to S-wave arrivals and are therefore easiest to identify. Knowledge of the velocities of P and S waves (i.e., V_P and V_S, respectively) passing through geological materials can be used to identify subsurface rock types. Thus, our measurements of values of V_P and V_S for this diverse suite of samples, under dry and wet conditions, will facilitate interpretation of seismic sections for which subsurface velocity structures have been derived via inversion.

The values of ultrasonic P-wave velocities (V_P) are most important to the ongoing seismic surveys, since inversions of the seismic-survey data are based mainly on V_P. Values of S-wave velocities (V_S) are more difficult to carry out inversions for, but they are useful for refining interpretations of seismic profiles. The distribution of pore fluids and pore-fluid pressures in the subsurface of the Nechako Basin are unknown but are unlikely to be negligible. Furthermore, pore-fluid pressure exerts a significant influence on seismic reflection. On this basis, we elected to make both 'Dry' and 'Wet' (i.e., water-saturated) ultrasonic measurements of V_P and V_S for each sample core.

The P- and S-wave arrival times for sample cores were measured using a bench-top apparatus at EOST. Measurements were made using an Agilent Technologies model DSO5012A digital-storage oscilloscope, an Agilent Technologies model 33210A 10 MHz function/waveform generator, and two broadband PZT piezoelectric transducer crystals (100 kHz to 1 MHz frequency), one located at each end of the sample. Measurements were made under a stress of approximately 1 MPa to ensure good contact between the instrument's end caps and the polished ends of the sample core. The P-wave measurements were based on a transmitted frequency of 700 kHz; S-wave measurements used a frequency of 300 kHz. The P-wave arrivals were chosen as the first clearly identified signal following the triggering pulse from the function generator. The S-arrival is characterized by a distinct change in the ultrasonic response of the sample with time. The onsets of the S-wave arrivals were determined by identifying the first significant change in signal amplitude or the first distinct inflection point in the slope of the signal following the P-wave arrival.

Derivative (Computed) Properties

The measured values of V_P and V_S for cores of rock samples allow the calculation of derivative properties, namely several elastic (dynamic) properties (Table 2). In this section, we review the calculation of Poisson's ratio and Young's modulus (Tables 2 and 3).

Elastic compression and extension are described by Hooke's Law,

$$\sigma = E \cdot \varepsilon, \tag{5}$$

where σ is the normal stress and ε is the elongation or normal strain. Young's modulus (E) is the measure of stiffness and is traditionally taken as the ratio between the tensile stress and tensile strain. Here, we define E as the ratio of uniaxial stress to uniaxial strain. Young's modulus calculated from ultrasonic velocities is an indirect and nondestructive way of determining the stiffness of rock samples. For most rocks, E has values between 10 and 200 GPa (Telford et al., 1976).

Poisson's ratio is the ratio between the shortening and expansion of a material under uniaxial compression. Most rocks have Poisson's ratios between 0.05 (for very hard, rigid rock) to 0.45 (for soft, poorly consolidated material; Telford et al., 1976).

Using ultrasonic measurements of P- and S-wave velocities, the dynamic elastic moduli can be computed for Poisson's ratio (υ_d) as

$$\upsilon_d = \frac{V_P^2 - 2V_S^2}{2(V_P^2 - V_S^2)} \tag{6}$$

and for Young modulus (E_d) as

$$E_d = \rho \times \left[\frac{V_S^2 (3V_P^2 - 4V_S^2)}{V_P^2 - V_S^2} \right], \tag{7}$$

where ρ is the bulk density of the sample (g/cc).

Results

We describe in this section the experimental results obtained for each of the six lithostratigraphic packages (Ta-

bles 1 and 3). The range of values measured for the various properties across all lithostratigraphic packages is extreme (Table 3):

- porosity: 0.15–30.06%
- density: 2.45–3.02 g/cc
- chargeability: 0.0–55.6 ms
- NRM: 1.0–48.0
- resistivity: 46–95646 Ω•m
- magnetic susceptibility: 0.01–0.11 SI
- dry V_P: 1.65–6.17 km/s
- dry V_S: 1.04–4.04 km/s
- wet V_P: 3.02–6.63 km/s
- wet V_S: 1.47–4.10 km/s

Variation within lithostratigraphic packages is substantially less and reflects the physical and lithological variations within each package. Some packages comprise a narrow range of rock types (e.g., Miocene Chilcotin basalts [CB]) and can show a correspondingly narrow range of physical and geophysical properties (Table 3). Other lithostratigraphic packages comprise a diverse range of rock types (e.g., Eocene volcanic and sedimentary rocks [EVS]) and show a correspondingly wide range of properties. Ultimately, this extensive and high-quality dataset is intended for Geoscience BC's digital database and promises to facilitate geophysical interpretations of the geology in the Nechako Basin region of central BC. Data from each of the six lithostratigraphic packages have been plotted on

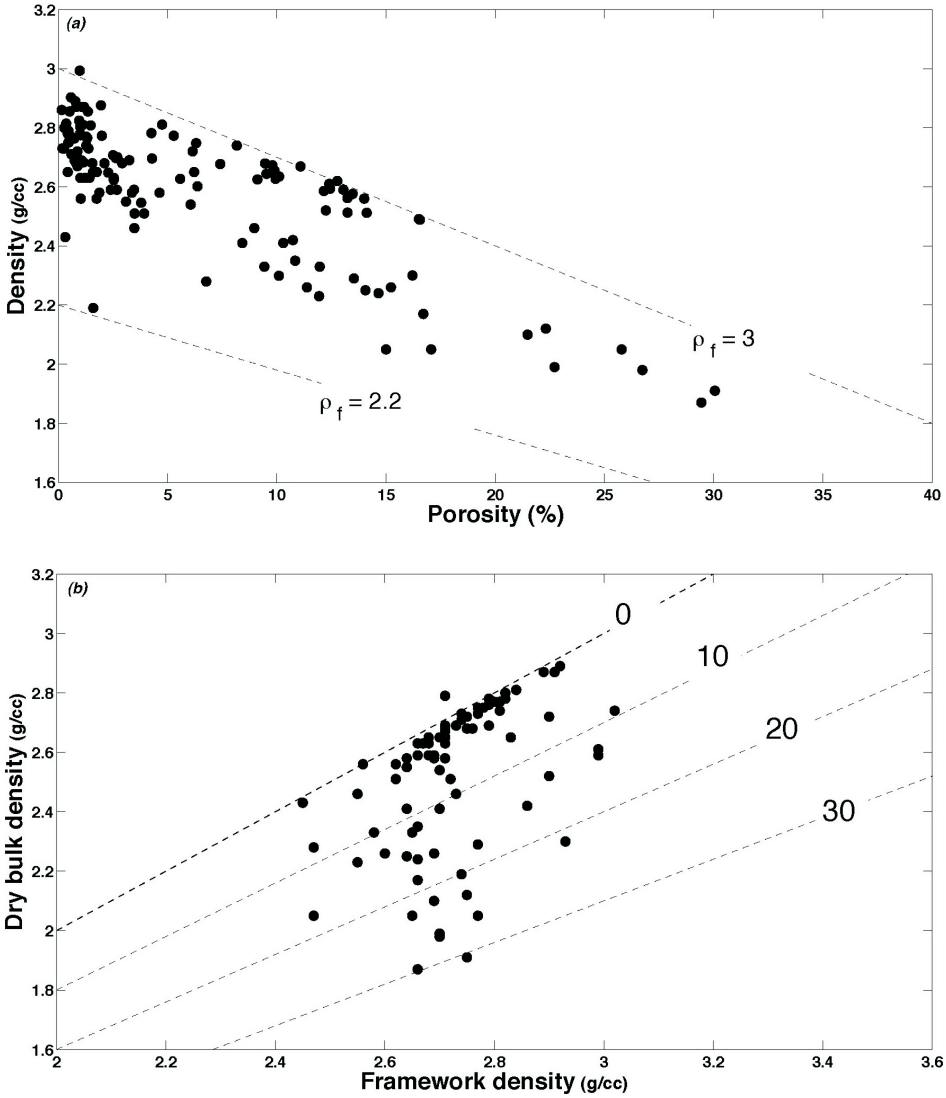

Figure 3. Density and porosity ranges for the entire suite of samples collected within the Nechako Basin: **a)** measured values of dry bulk density plotted versus porosity, ranging from 0% to 30%, confirming the expected negative correlation; the broad trend described by the dataset lies between model density–porosity lines for samples having framework density (ρ_f) values of 2.2 and 3 g/cc; **b)** measured values of bulk density and framework density, which varies from ~2.4 to 3.1 g/cc and represents the skeletal density plus any isolated pore space (<1% in these samples); contours map the decrease in bulk density due to increasing porosity (%).

multiparameter diagrams (Table 3) to characterize the within-package variations in physical properties.

As part of our physical-property characterization of the samples, we measured bulk and framework densities and porosity. Many geophysical properties are, themselves, dependent on or sensitive to these physical properties. The suite of 167 samples has a porosity range of 0–30 vol. % (Figure 3a); the porosity is assumed to be fully connected. On the basis of the different methods used to measure density, we saw no evidence for a substantial fraction of isolated porosity. Bulk density (rock plus pore space) ranges from ~1.8 to 3.0 g/cc, whereas the corresponding framework density varies between ~2.4 and 3.0 g/cc. The relationship between bulk and framework density and porosity is illustrated in Figure 3b. At zero porosity, bulk and framework density are equivalent. The contours in Figure 3b illustrate the effect of porosity in reducing the bulk density of samples relative to their framework density.

The magnetic properties of the six lithostratigraphic packages are shown in Figure 4 (Table 3; Figure 4a–f). The K_N values for the entire suite vary over four orders of magnitude, from 10^{-2} to 10^{2}. Magnetic susceptibility varies over three orders of magnitude, from 10^{-4} to 10^{-1} ms. High values of K_N indicate rocks that have preserved the magnitude and direction of the global magnetic field at the time of emplacement. For samples having high values of K_N (>1), the measured values of magnetic susceptibility need to be corrected in order to use the data to identify and interpret magnetic anomalies. Within the Nechako Basin, K_N is a relatively good indicator of volcanic rocks emplaced at elevated temperature (exhibiting thermoremanent NRM), whereas sedimentary rocks have low K_N values. In most rocks, variations in *k* mainly reflect modal variations in magnetic minerals (particularly magnetite; Telford et al., 1976). However, given the large variability of *k* within rock types and the significant overlap in *k* values across rock types, *k* is, by itself, a poor discriminator of lithostratigraphic packages. The Chilcotin basalts are characterized by high K_N values (~1–100), and their *k* values vary over three orders of magnitude. The EVS package has very similar ranges of K_N and *k*, although fewer samples were measured. The KVS rocks show a greater range in K_N and have a lower mean value, while showing an identical variation in *k*. The wide range of K_N values for the KVS package indicates a broad range of rock types incorporated into this package. The JS samples are distinguished by low values of K_N and restricted and low values of *k*. This reflects the fact that they are dominantly sedimentary in provenance. Con-

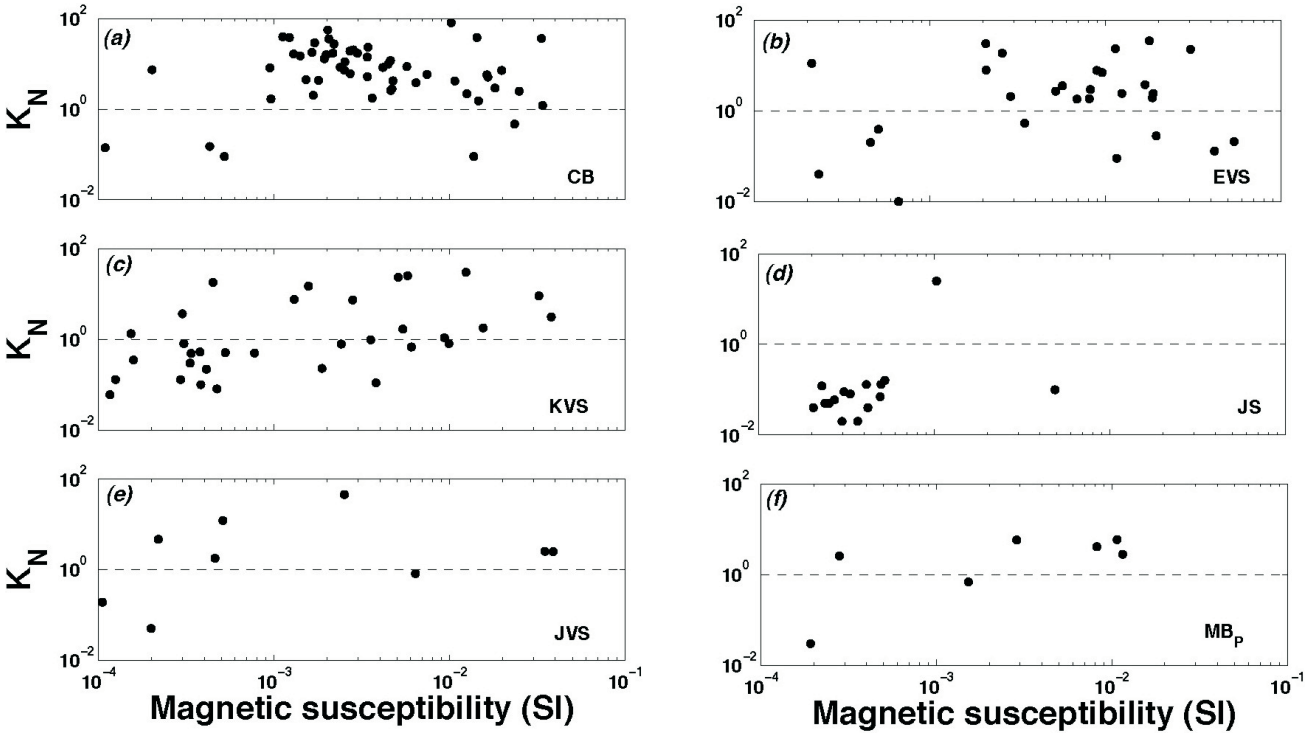

Figure 4. Relationship between K_N (Koenigsberger ratio) and magnetic susceptibility for the lithostratigraphic packages listed in Table 1: **a)** Chilcotin Group basaltic lavas (CB), **b)** Eocene volcanic and sedimentary rocks (EVS), **c)** Cretaceous volcaniclastic and sedimentary rocks (KVS), **d)** Middle–Late Jurassic sedimentary rocks (JS), **e)** Lower–Middle Jurassic volcanic and sedimentary rocks (JVS), and **f)** Mesozoic basement rocks (MB_p). The dashed lines at $K_N = 1$ indicate the threshold above which the magnetic-anomaly interpretation needs to be corrected for remanent magnetization (NRM; see text); the data presented are not corrected for NRM. For example, nearly all CB basalts have K_N values >1 and require corrections to the experimentally measured values of magnetic susceptibility. Conversely, JS samples are largely unaffected by NRM.

versely the small numbers of samples within the JVS package suggest wide-ranging K_N and k properties similar to those observed in the EVS and KVS packages. The basement rocks (MB_p) have intermediate to low K_N and a range of k values. These properties are largely a reflection of the variable modal mineralogy of the plutonic rocks collected to represent the basement to the Nechako Basin.

The resistivity values for each lithological package are plotted as a function of sample porosity (Figure 5). Figure 5a demonstrates clearly that the range of resistivities in CB (127–95 646 Ω·m) is controlled by mineralogical composition and has very little dependence, if any, on sample porosity. The CB rocks are relatively lithologically homogeneous but vary widely in porosity (~0–17%) due to their varying vesicularity. This wide range of porosity has no apparent effect on the resistivity of the CB sample package. Conversely, the variation in sample resistivity of two orders of magnitude seen in these basalts is likely a reflection of variations in crystallinity, grain size and bulk mineralogy. The EVS sample package (Figure 5b) clearly shows a decrease in resistivity by three orders of magnitude (from approximately 10^4 to 10^1 Ω·m) as a function of porosity. This sample package is more lithologically varied and, although there is some variation in resistivity at constant porosity, the emergent trend demonstrates that mineralogy and bulk composition are likely secondary contributors to resistivity. The resistivity of the KVS sample package decreases more than two orders of magnitude (from 10^4 to 10^2 Ω·m) with porosity (Figure 5c), a variation that is less pronounced than in the EVS package . This may suggest that both composition and porosity control resistivity in this lithostratigraphic package. The JS package shows a resistivity range of two orders of magnitude (from 10^4–10^2 Ω·m) over a change of less than 5% in porosity (Figure 5d). The tight clustering of data suggests that JS rocks can be discriminated from other package s on the basis of measured porosity and resistivity. Resistivity of the JVS sample package decreases with increasing porosity (Figure 5e). As this package is lithologically uniform, it is expected that most variation in resistivity (10^4–10^2 Ω·m) is porosity controlled. Lastly, the relatively homogeneous lithology and generally low porosity of the basement rocks (MB_p) results in a tight clustering of data (Figure 5f) similar to that observed for the JS rocks. In every case where porosity variation is large, save for the CB package, resistivity decreases with increasing porosity.

The ranges of values for resistivity and chargeability are organized by lithostratigraphic package (with the exception

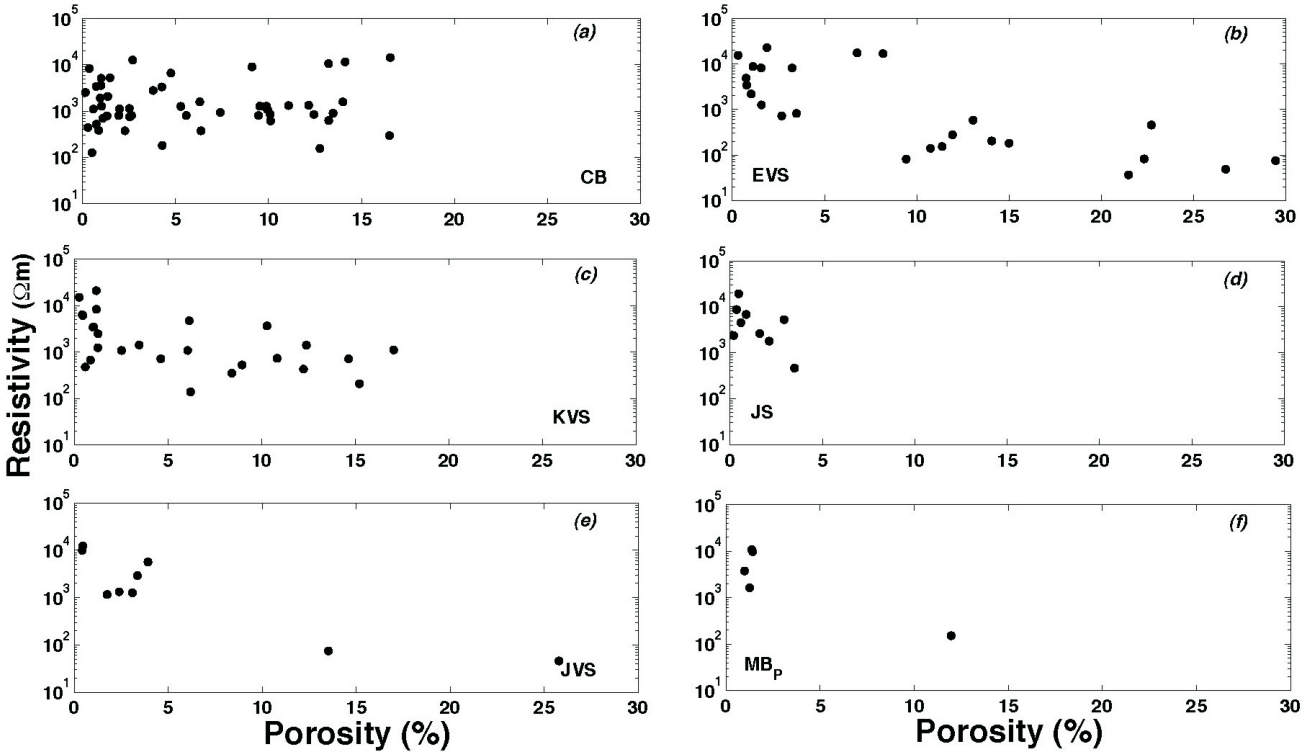

Figure 5. Experimentally measured values of resistivity (Table 2) plotted against total porosity of each sample for the lithostratigraphic packages listed in Table 1: **a)** Chilcotin Group basaltic lavas (CB), **b)** Eocene volcanic and sedimentary rocks (EVS), **c)** Cretaceous volcaniclastic and sedimentary rocks (KVS), **d)** Middle–Late Jurassic sedimentary rocks (JS), **e)** Lower–Middle Jurassic volcanic and sedimentary rocks (JVS), and **f)** Mesozoic basement rocks (MB_p). Resistivity commonly decreases with porosity (cf. parts b–f). Samples of CB show two orders of magnitude variation in resistivity that does not correlate with porosity, the implication being that resistivity in these basalts is controlled by variations in crystallinity, grain size or bulk mineralogy.

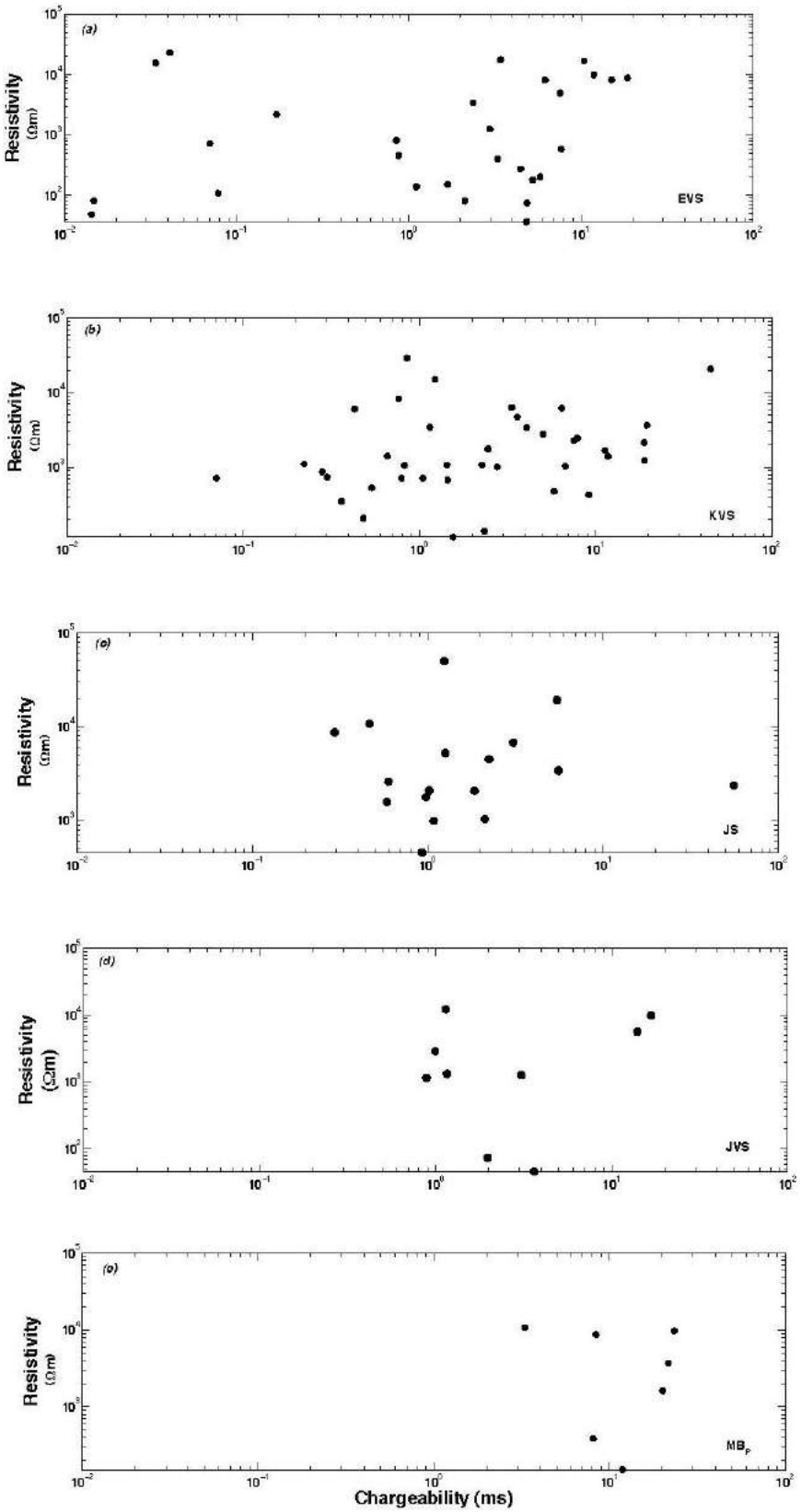

Figure 6. Experimentally measured values of resistivity and chargeability (Table 2) plotted for all lithostratigraphic packages listed in Table 1: **a)** Eocene volcanic and sedimentary rocks (EVS), **b)** Cretaceous volcaniclastic and sedimentary rocks (KVS), **c)** Middle–Late Jurassic sedimentary rocks (JS), **d)** Lower–Middle Jurassic volcanic and sedimentary rocks (JVS), and **e)** Mesozoic basement rocks (MB_p).

of CB) in Figure 6a–e. The resistivity range of EVS (Figure 6a) is less than three orders of magnitude, and chargeability varies by as much as four orders of magnitude. This broad range of values is largely controlled by lithology, although enhanced by the wide range of porosity in the EVS sample package. Resistivity measurements were conducted under distilled water–saturated conditions. Such conditions are expected to dissolve any late-stage groundwater-derived mineral precipitates lining the pore spaces, thereby creating ionic pore fluids and a more conductive sample. However, as shown in Figure 5, resistivity decreases with increasing preserved porosity, suggesting a paucity of such mineral precipitates in these pore spaces. Likewise, KVS (Figure 6b) also demonstrates a broad range of resistivities and chargeabilities, testament to the broad range in lithology and variation in porosity of the sample package. The JS sample package (Figure 6c) ranges in resistivity and chargeability across two and a half orders of magnitude. The resistivity range of JVS (Figure 6d) is approximately 2.5 orders of magnitude, whereas the chargeability range of this package is slightly greater than one order of magnitude. The tighter range of chargeability values for both JS and JVS is controlled predominantly by lithology. Lithological variation within each package is limited, suggesting that any scatter in resistivity is due to porosity. The porosity of the JS package rocks is negligible compared to that of the JVS package, suggesting that the narrower range of resistivities within the JS package is lithologically controlled. Figure 6e shows the ranges in resistivity (approximately two orders of magnitude) and chargeability (approximately one order of magnitude) for the MB_p rocks. This package contains lithologically similar rocks (plutonic rocks) of relatively low porosity, ensuring that the range in measured electrical properties is small.

The seismic properties of the Nechako Basin sample suite are possibly the most useful for package discrimination. Figure 7 displays the P-wave velocity (V_P) of the Chilcotin basalts (CB) as a function of sample density under various confining pressures. Dashed lines indicate the corresponding porosities for all samples. It is clear that V_P increases with decreasing porosity and increasing confining pressure; V_P is therefore highest for stronger, low-porosity rocks. With increasing confining pressure, V_P increases as pore space is closed and the rock becomes more coherent.

Figure 8a–e shows the dry and wet V_P and V_S values for the EVS, KVS, JS, JVS, and MB_p lithological packages. Dry samples have lower V_P/V_S values (1.5-2) than water saturated samples (1.75-3). Dashed lines indicate V_P/V_S ratios of 1, 1.5, 2 and 3. Wet V_P/V_S ratios for all packages (1.75–3) are consistently higher than the same ratios calculated for dry samples (1.5–2; O'Connell and Budiansky, 1974). Figure 8a (EVS), 8b (KVS) and 8d (JVS) shows the most variation in V_P/V_S ratios (1.5–3 for EVS and KVS), testament to the variable lithology in each package (which includes both volcanic and sedimentary rocks of varying porosity). Ratios for the JS (Figure 8c) and MB_p (Figure 8e) packages are relatively well constrained between 1.5 and 2. Ratios of V_P:V_S have been demonstrated to be strong indicators of variations in fluid-saturation conditions within rocks

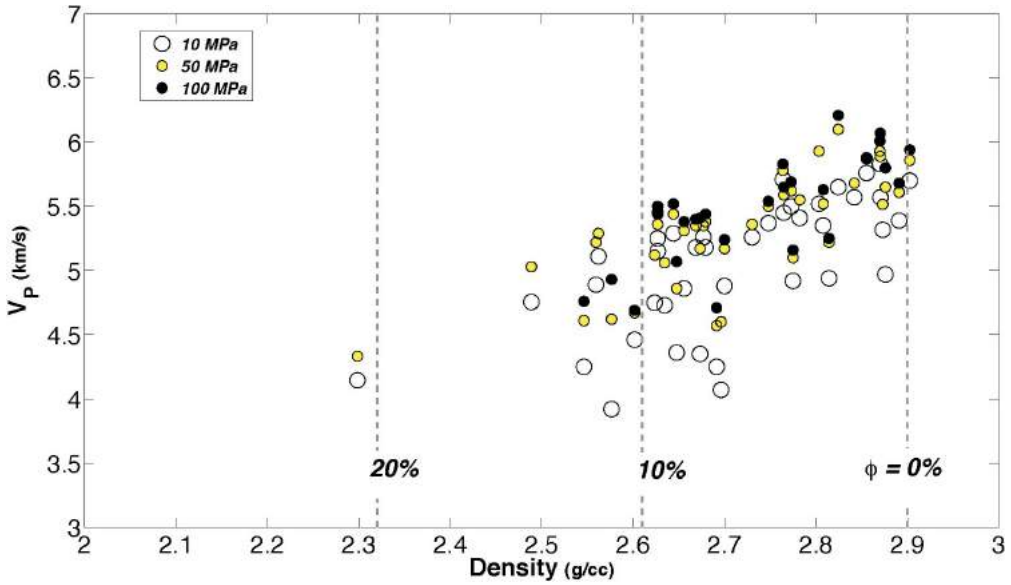

Figure 7. Plot of compressional-wave (P-wave) velocity (V_P) versus bulk density for core samples of Chilcotin basalts. Both V_P and density are measured on dry, as opposed to water-saturated, sample cores. Values of V_P are measured under load pressures of 10, 50 and 100 MPa. Dashed lines denote model values of density for samples having total porosities (ϕ) of 0%, 10% and 20%, and assuming a skeletal density of 2.9 g/cc. Values of V_P increase with increasing confining pressure (i.e., load) and decrease with decreasing porosity (increasing density).

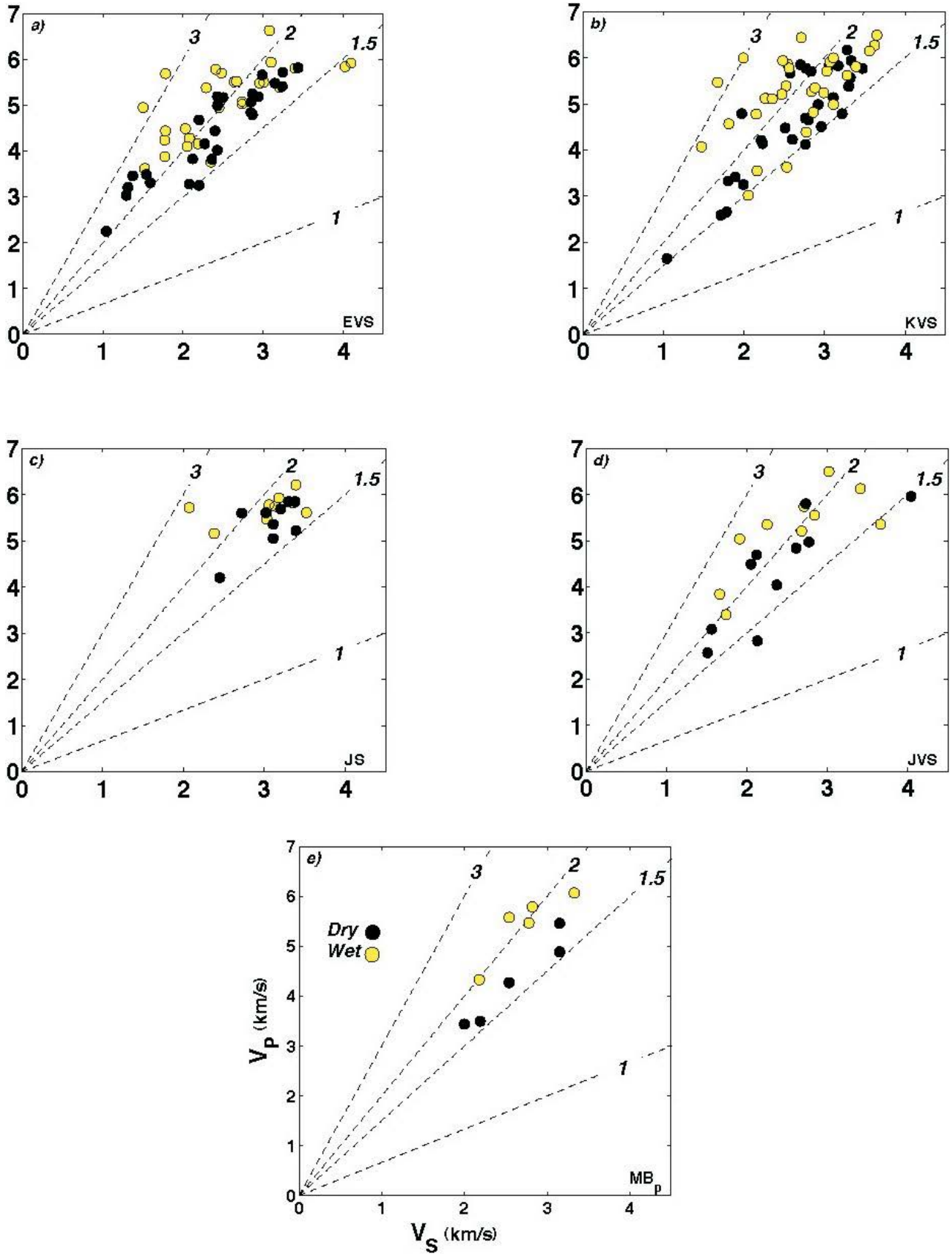

Figure 8. Plots of compressional-wave velocity (V_P) versus shear-wave velocity (V_S) measured on dried (black symbols) and water-saturated (yellow symbols) cores taken from all samples (Table 2) except the CB package . Diagram is contoured for ratios of V_P/V_S of 1, 1.5, 2 and 3.

(O'Connell and Budiansky, 1974). On this basis, further investigation of seismic velocities within the Nechako Basin could elucidate both density of crack distributions within the underlying stratigraphy and, more importantly, the degree of fluid saturation of these cracks. The latter (e.g., fluid distribution) relates directly to our capacity to assess the hydrocarbon potential of the basin.

Figures 9–13 show the dependence of both dry and wet ultrasonic velocities on bulk density and porosity, and the dependence of dry and wet elastic moduli on porosity. For all figures, (a) plots wet and dry P-wave velocities as a function of density; (b) plots wet and dry S-wave velocities as a function of density; (c) plots wet and dry P-wave velocities as a function of porosity; (d) plots wet and dry P-wave velocities as a function of porosity; (e) plots wet and dry Young's modulus as a function of porosity; and (f) plots wet and dry Poisson's ratio as a function of porosity. All dry ultrasonic velocities are plotted against dry bulk densities; likewise, all wet ultrasonic velocities are plotted as functions of their wet bulk densities. Each figure deals with a different package of rocks.

The same relationships are observed in all plots (Figures 9–13), although those packages with both larger sample suites and greater heterogeneity in bulk density and porosity display these relationships more clearly. Figures 9a–13a and 9b–13b exhibit increasing ultrasonic velocity with increasing sample bulk density. Conversely, although perhaps intuitively, these same ultrasonic velocities decrease with increasing porosity (Figures 9c–13c and 9d–13d). The presence of dry void space or water-saturated void space affects both P- and S-wave velocities considerably for all rocks (O'Connell and Budiansky, 1976). Most samples exhibit higher ultrasonic velocities when saturated in water, and this becomes more pronounced with increasing porosity. Elastic moduli are frequency dependent (Walsh, 1965; O'Connell and Budiansky, 1976) and sensitive to sample saturation, which increases seismic velocity. Figures 9e–13e show that the Young's modulus of all rocks decreases with porosity, reflecting decreasing stiffness (Walsh, 1965). Poisson's ratio is the ratio between transverse strain to longitudinal strain and can be estimated from the velocities of compressional (longitudinal) and shear (transverse)

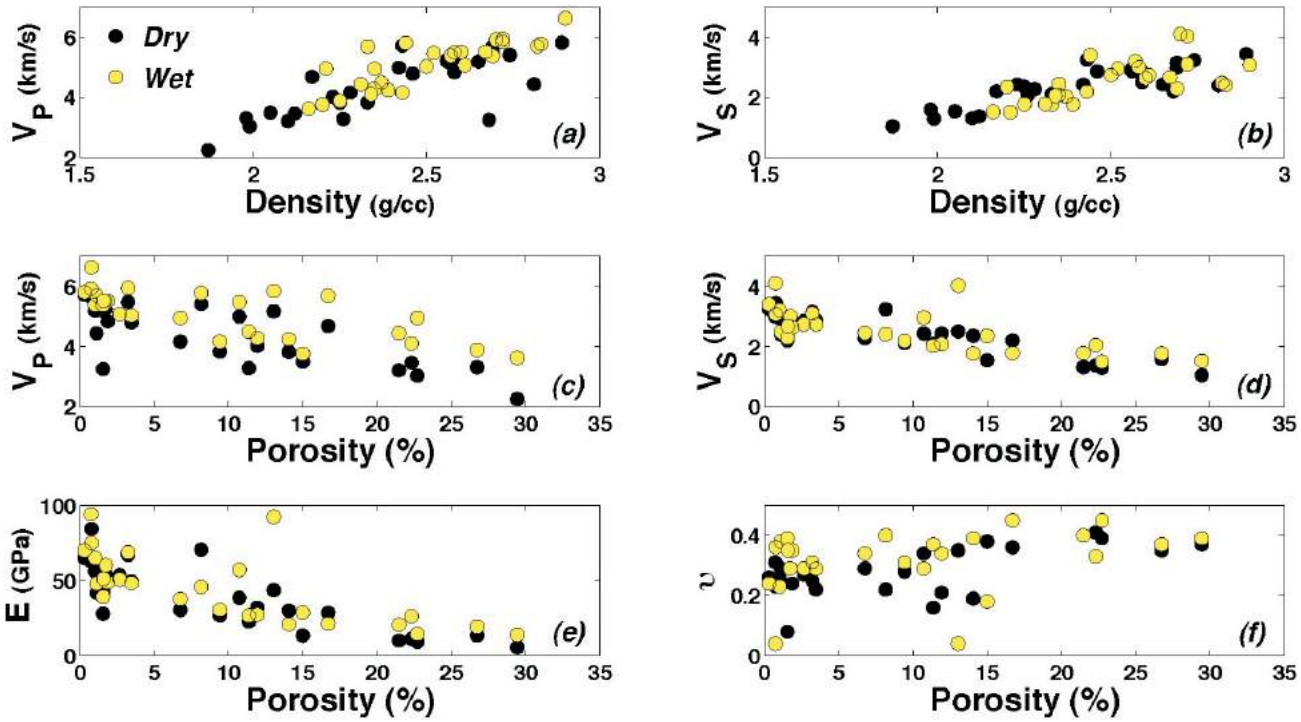

Figure 9. Dependence of dry and wet ultrasonic velocities on bulk density and porosity, and dependence of dry and wet elastic moduli on porosity for Eocene volcanic and sedimentary rocks (EVS; Table 3): **a)** V_P as a function of bulk density; **b)** V_S as a function of bulk density; **c)** V_P as a function of connected porosity; **d)** V_S as a function of connected porosity; **e)** dynamic Young's modulus (E_d) as a function of connected porosity; **f)** Poisson's ratio (υ), calculated from measured values of V_P and V_S, as a function of connected porosity. In parts (a) and (b), dry ultrasonic velocities are plotted against dry bulk densities, and wet ultrasonic velocities against wet bulk densities. Values of V_P and V_S increase with bulk density and decrease with porosity. Young's Modulus decreases with increasing porosity due to the inherent weakness of porous rock. V_P and V_S and moduli are consistently larger for water-saturated samples than for dry samples.

waves. Figures 9f–13f show that there appears to be little relationship between the calculated Poisson's ratios and porosities of the six Nechako Basin packages.

Geophysical Discrimination within the Nechako Basin

In this section, we develop a decision table (Table 4) to facilitate geophysical discrimination of lithostratigraphic units in the subsurface to the Nechako Basin. We highlight the most reliable indices for discrimination between the six major lithostratigraphic packages described in Table 1. Each cell in Table 4 contains physical properties appropriate for distinguishing between the units of the intersecting column and row. This is not an exhaustive set of discriminators. In part, the decision table reflects, and is limited by, the fact that we have packaged the rocks on the basis of age, geography and lithology.

The Miocene Chilcotin basalts (CB) are one of the most distinctive lithostratigraphic packages underlying the Nechako Basin. These rocks have higher dry V_p values (4.2–6.0 km/s) than the range of values observed for the Eocene volcanic and sedimentary (EVS) package (2.2–5.8 km/s). The V_p values for CB rocks (4.2–6.0 km/s) overlap those measured for Cretaceous volcaniclastic and sedimentary (KVS) rocks (1.6–6.2 km/s) but are generally higher; the overlap is a reflection of the diverse range of V_p values within the KVS package. The CB package is easily distinguished from rock types within the Middle–Late Jurassic sedimentary (JS) package on the basis of NRM. The CB package shows a large range of values from below detection (b.d.) to 48 A/m; in contrast, the JS rocks have a limited range (b.d. to 1.0 A/m), and most samples have NRM values of <0.1 A/m. Distinguishing CB rocks from rocks of the Lower–Middle Jurassic volcanic and sedimentary (JVS) package is more uncertain. The dry V_p offers partial discrimination of CB (4.2–6.0 km/s) from JVS (2.5–5.9 km/s), in that CB rocks have V_p values restricted to the upper range of JVS values. The difficulty in discriminating between these two lithostratigraphic packages reflects the lithological diversity of the JVS package and the fact that it contains many similar volcanic rocks. Similarly, CB rocks are poorly distinguished from the Mesozoic basement rocks (MB_p), although they have a higher mean V_p (4.2–6.0 km/s) than the MB_p package (3.4–5.5 km/s).

The EVS package is indistinguishable from the KVS package in terms of all the measured geophysical properties: this is not surprising, given that the lithological make-up of both packages is very similar. The sole distinguishing prop-

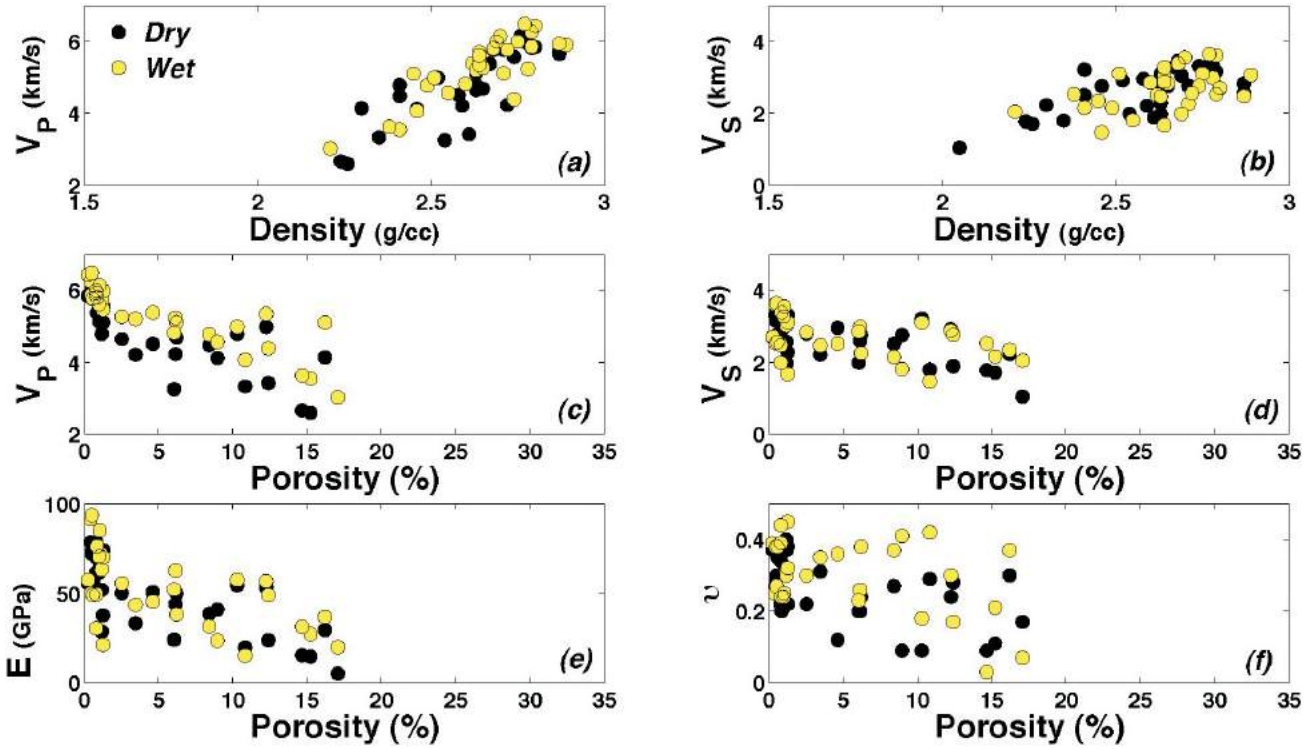

Figure 10. Dependence of dry and wet ultrasonic velocities on bulk density and porosity, and dependence of dry and wet elastic moduli on porosity for Cretaceous volcaniclastic and sedimentary rocks (KVS; Table 3): **a)** V_P as a function of bulk density; **b)** V_S as a function of bulk density; **c)** V_P as a function of connected porosity; **d)** V_S as a function of connected porosity; **e)** dynamic Young's modulus (E_d) as a function of connected porosity; **f)** Poisson's ratio (υ), calculated from measured values of V_P and V_S, as a function of connected porosity. In parts (a) and (b), dry ultrasonic velocities are plotted against dry bulk densities, and wet ultrasonic velocities against wet bulk densities. Values of V_P and V_S increase with bulk density and decrease with porosity.

erty is porosity: the EVS package has higher porosity (~30%) than the KVS package, which is consistently less than 17%. Although not ideal, this is the only viable way of distinguishing between the EVS and KVS packages. Rocks of the EVS package are easily distinguished from those of the JS package in the following ways: 1) NRM values for EVS rocks (b.d. to 28 A/m) are substantially higher than those of JS rocks (most are <0.004 A/m); 2) values of chargeability (m_T) can also help distinguish EVS (b.d. to 19 ms) from JS (0.3–56 ms); 3) values of dry and water-saturated V_p values overlap, but EVS rocks (2.35–5.8 and 3.6–6.6 km/s) show a greater range than JS rocks (4.2–5.8 and 5.2–6.2 km/s); 4) on average, EVS rocks are less resistive (37–23 035 Ω·m) than JS rocks (460–49 883 Ω·m), but there is complete overlap between the ranges. As with KVS rocks, JVS rocks cannot be reliably distinguished from EVS rocks by any geophysical property reported; this is due to the similar lithological components in each package. The EVS rocks are also poorly distinguished from MB_p rocks, although all MB_p geophysical-property ranges are narrower and lie completely within EVS ranges. This is due to the variety of rock types within the EVS package, which also includes some igneous samples.

As with the EVS package, it is difficult to distinguish the various lithological packages from the Cretaceous volcanic and sedimentary (KVS) package. Discrimination is hindered by the variety of rock types grouped under the KVS label, which has resulted in a large scatter of geophysical-property data. There is poor distinction between KVS and JVS, since both packages encompass similar rock types, although resistivity has potential as a geophysical discriminator. The resistivity ranges of both packages overlap considerably, although KVS resistivities (116–29 011 Ω·m) are consistently higher than those characterizing the JVS package (46–12 338 Ω·m). There is significant overlap between KVS and JVS ultrasonic velocities, rendering these two packages seismically indistinguishable. As with the EVS package, NRM values for KVS (b.d. to 15.1 A/m) are substantially higher than those of JS rock units (most are <0.004 A/m). Ultrasonic velocities of KVS rocks vary greatly due to lithological diversity in this package. However, JS rocks are both lithologically and physically similar (porosities are <3.5%), resulting in narrow ranges for their seismic velocities (V_{PDry}^{JS} of 4.2–5.8 km/s; V_{SDry}^{JS} of 2.4–3.4 km/s), which are consistently much higher than those of

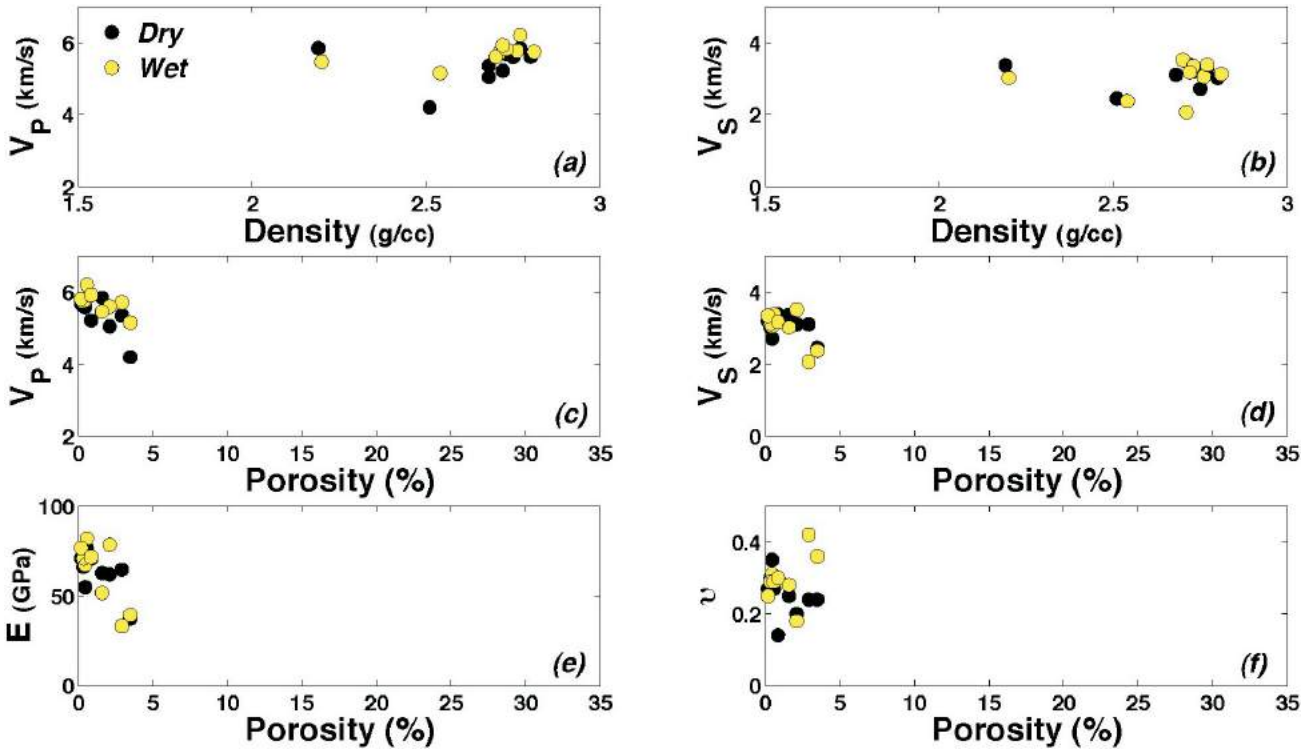

Figure 11. Dependence of dry and wet ultrasonic velocities on bulk density and porosity, and dependence of dry and wet elastic moduli on porosity for Middle–Late Jurassic sedimentary rocks (JS; Table 3): **a)** V_P as a function of bulk density; **b)** V_S as a function of bulk density; **c)** V_P as a function of connected porosity; **d)** V_S as a function of connected porosity; **e)** dynamic Young's modulus (E_d) as a function of connected porosity; **f)** Poisson's ratio (υ), calculated from measured values of V_P and V_S, as a function of connected porosity. In parts (a) and (b), dry ultrasonic velocities are plotted against dry bulk densities, and wet ultrasonic velocities against wet bulk densities.

KVS (V_{PDry}^{KVS} of 1.6–6.2 km/s; V_{SDry}^{KVS} of 1.0–3.5 km/s). The ranges of all physical properties for MB_p rocks are consistently narrower than for KVS rocks, due to the compositional and physical similarity of all the basement rocks. However, the ranges of values for every measured geophysical property of MB_p rocks lie within the broader ranges of properties of the KVS package. Geophysical identification of MB_p rocks in the subsurface thus requires the use of all properties.

Jurassic sedimentary (JS) rocks are poorly distinguished from the Jurassic volcanic and sedimentary (JVS) package, but resistivity values may offer some potential. Although there is overlap in resistivity values between JS and JVS, resistivities of JS rocks (460–49 883 Ω·m) are consistently higher than those of JVS rocks (46–12 338 Ω·m). The ranges of all physical properties for MB_p are consistently narrower than those for JVS rocks but are fully enclosed by the large ranges of the JVS package. It is recommended that all the available properties be used when identifying MB_p rocks in the subsurface.

Both the JS and MB_p packages represent lithologically well-defined rock packages that populate distinct geophysical-property ranges, which makes their distinction relatively easy compared to other packages. Their ranges in resistivity and seismic velocity have relatively little overlap and are the most useful properties for discrimination. The resistivity range for JS rocks is 460–49 883 Ω·m, which is considerably higher than that for MB_p (152–10 771 Ω·m). Ultrasonic velocities also offer adequate discrimination because JS velocities (V_{PDry}^{JS} of 4.20–5.85 km/s; V_{SDry}^{JS} of 2.45–3.39 km/s) are higher than those of MB_p rocks (V_{PDry}^{MBp} of 3.44–5.46 km/s; V_{SDry}^{MBp} of 2.00–3.15 km/s).

Summary

The Nechako Basin represents one of the most challenging areas for mineral and oil exploration in British Columbia. The challenge is that the basin is likely to be underlain by stratigraphically and structurally complex geology. This complexity is exacerbated by the fact that the quality and distribution of bedrock exposure is highly variable; overall, the exposure is poor throughout the region. In addition, only a limited amount of knowledge of the subsurface geology has been derived from previous oil-exploration efforts. These early oil-exploration efforts provided few drillholes and geophysical surveys. However, the last decade has seen a tremendous increase in new knowledge derived from mapping (e.g., Riddell, 2006, 2011; Dohaney et al., 2010; Andrews et al., 2011; Bordet and Hart, 2011) and multi-

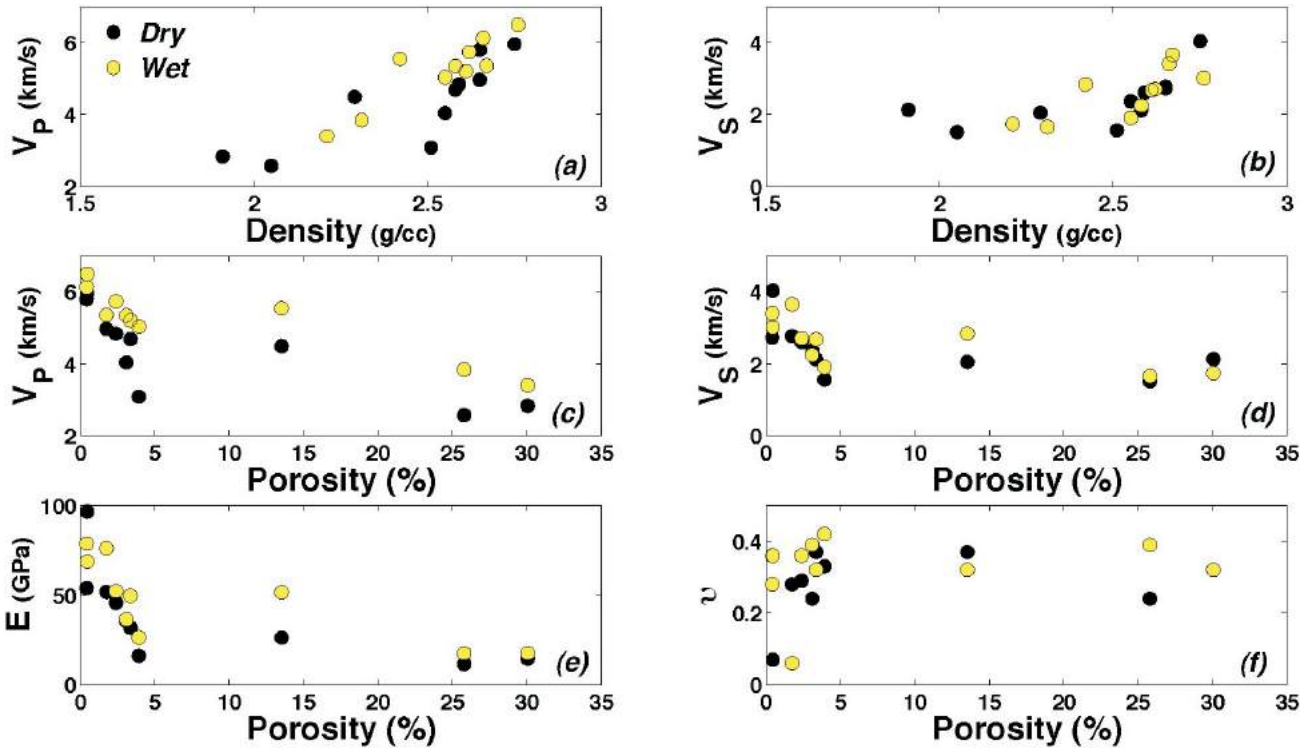

Figure 12. Dependence of dry and wet ultrasonic velocities on bulk density and porosity, and dependence of dry and wet elastic moduli on porosity for Lower–Middle Jurassic volcanic and sedimentary rocks (JVS; Table 3): **a)** V_P as a function of bulk density; **b)** V_S as a function of bulk density; **c)** V_P as a function of connected porosity; **d)** V_S as a function of connected porosity; **e)** dynamic Young's modulus (E_d) as a function of connected porosity; **f)** Poisson's ratio (υ), calculated from measured values of V_P and V_S, as a function of connected porosity. In parts (a) and (b), dry ultrasonic velocities are plotted against dry bulk densities, and wet ultrasonic velocities against wet bulk densities.

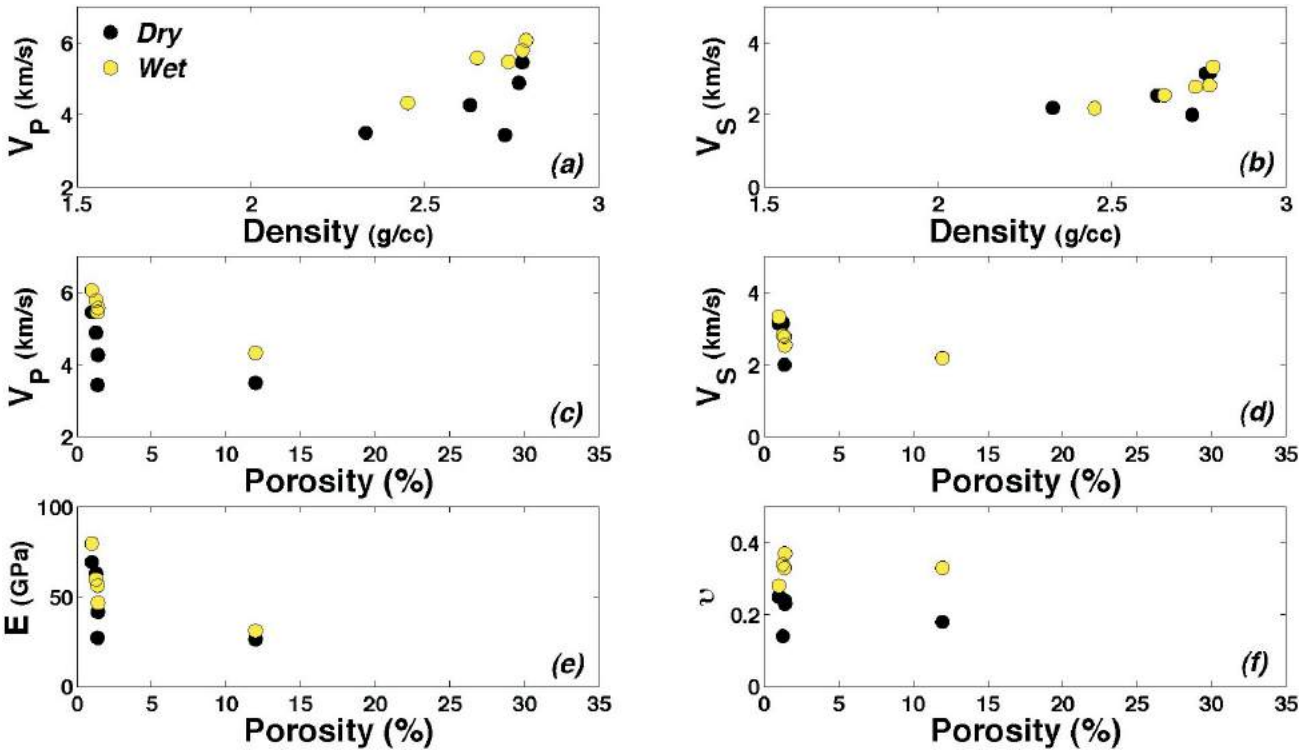

Figure 13. Dependence of dry and wet ultrasonic velocities on bulk density and porosity, and dependence of dry and wet elastic moduli on porosity for Mesozoic basement rocks (MB_p; Table 3): **a)** V_P as a function of bulk density; **b)** V_S as a function of bulk density; **c)** V_P as a function of connected porosity; **d)** V_S as a function of connected porosity; **e)** dynamic Young's modulus (E_d) as a function of connected porosity; **f)** Poisson's ratio (υ), calculated from measured values of V_P and V_S, as a function of connected porosity. In parts (a) and (b), dry ultrasonic velocities are plotted against dry bulk densities, and wet ultrasonic velocities against wet bulk densities.

parameter geophysical surveys (e.g., Hayward and Calvert, 2011; Idowu et al., 2011; Spratt and Craven, 2011).

The range of possible geophysical responses from subsurface stratigraphic packages must be known in order to extract the maximum information from these large-scale field-based geophysical campaigns. The project reported here was a field-supported experimental program designed to measure a broad range of physical and geophysical properties of rock samples representing the lithostratigraphic diversity of the subsurface to the Nechako Basin. We sampled more than 11 major formations or mappable stratigraphic units (Table 1; Figure 2) across an area of >50 000 km^2 (Figure 2).

Measurements were taken of the physical (e.g., density, porosity) and geophysical (e.g., chargeability, seismic velocity) properties of the sample suite, with the aim of providing data that would facilitate interpretation of geophysical surveys probing the Nechako Basin subsurface. The full range of measurements included bulk density, porosity, magnetic susceptibility, remanent magnetization, electrical resistivity, induced-polarization chargeability and seismic-wave velocities. Ranges of values were then determined for each

Table 4. Decision table for discrimination of stratigraphic packages within the Nechako Basin on the basis of physical and geophysical properties.

EVS	KVS	JS	JVS	MB_P	Stratigraphic package
V_p	V_p	NRM	V_p	V_p	**CB**
	φ	V_p; V_s; m_T; NRM	m_T; V_s	V_p; V_s; m_T; Res	**EVS**
		V_p; V_s; NRM; Res	Res	V_p; V_s; m_T; Res; NRM	**KVS**
			V_p; V_s; Res	V_p; V_s; m_T; Res; NRM; k	**JS**
				V_p; V_s; NRM; Res; m_T	**JVS**

Stratigraphic package abbreviations: EVS, Eocene volcanic and sedimentary rocks; KVS, Cretaceous volcaniclastic and sedimentary rocks; JS, Middle–Late Jurassic sedimentary rocks; JVS, Lower–Middle Jurassic volcanic and sedimentary rocks; MB_p, Mesozoic basement rocks

Rock property abbreviations: k, magnetic susceptibility; Res, resistivity; V_p, compressional wave (P-wave) velocity; V_s, shear wave (S-wave) velocit mT, chargeability; NRM, natural remanent magnetization; φ, porosity

of six lithostratigraphic packages created by combining stratigraphic units on the basis of age, lithology and geography. Our compilation culminated in a decision table that summarizes the best opportunities for discriminating stratigraphic packages within the subsurface. Some units are not easily distinguished (e.g., Eocene and Cretaceous sedimentary and volcanic rocks), but there is good potential for discriminating between several important stratigraphic packages (Chilcotin basalts and Cretaceous sedimentary and volcanic rocks). Henceforth, these data should be used in the interpretation and reinterpretation of Nechako Basin geophysical surveys, and correlated with new and existing boreholes.

Acknowledgments

This study was supported by Geoscience BC project grant 2008-028 and Geological Survey of Canada contract 23254-096844-001-VAN, awarded to JKR. We thank J. Riddell, B. Struik, M. Mihalynuk, K. MacLaurin and P. Mustard for providing their archived samples. Sample preparation at UBC was conducted by P. Van de Reep and H. Dhillon. H. Linton and A. Tkachyk performed the lab work at the Geological Survey of Canada. Figure 1 was created by F. Ma of Geoscience BC. The authors thank L. Porritt and S. Kolzenburg for peer review comments that helped clarify the paper.

References

Andrews, G., Quane, S., Enkin, R.J., Russell, K., Kushnir, A., Kennedy, L., Hayward, N., and Heap, M. (2011): Rock physical property measurements to aid geophysical surveys in the Nechako Basin oil and gas region, central British Columbia; Geoscience BC, Report 2011-6, 40 p. and Excel® database, URL <http://www.geosciencebc.com/s/2011-06.asp> [November 2011].

Andrews, G.D.M., Plouffe, A., Ferbey, T., Russell, J.K., Brown, S.R. and Anderson, R.G. (2011): The thickness of Neogene and Quaternary cover across the central Interior Plateau, British Columbia: analysis of water-well drill records and implications for mineral exploration potential; Canadian Journal of Earth Sciences, v. 48, p. 973–986.

Andrews, G.D.M. and Russell, J.K. (2007): Mineral exploration potential beneath the Chilcotin Group (NTS 092O, P, 093A, B, C, F, G, I, J, K), south-central British Columbia: preliminary insights from volcanic facies analysis; *in* Geological Fieldwork 2006, BC Ministry of Energy and Mines, Paper 2007-1 and Geoscience BC, Report 2007-1, p. 229–238, URL <http://www.empr.gov.bc.ca/Mining/Geoscience/PublicationsCatalogue/Fieldwork/Documents/22-Andrews.pdf> [November 2011].

Andrews, G.D.M. and Russell, J.K. (2008): Cover thickness across the southern Interior Plateau, British Columbia (NTS 092O, P; 093A, B, C, F): constraints from water-well records; *in* Geoscience BC Summary of Activities 2007, Geoscience BC, Report 2008-1, p. 11–20, URL <http://www.geosciencebc.com/i/pdf/SummaryofActivities2007/SoA2007-Andrews_original.pdf> [November 2011].

Bordet, E. and Hart, C.J.R. (2011): Characterization and structural framework of Eocene volcanic sequences in the Nechako region, central British Columbia (NTS 092N, O, 093B, C, G); *in* Geoscience BC Summary of Activities 2010, Geoscience BC, Report 2011-1, p. 239–254, URL <http://www.geosciencebc.com/i/pdf/SummaryofActivities2010/SoA2010_Bordet&Hart.pdf> [November 2011].

Calvert, A.J., Hayward, N., Smithyman, B.R. and Takham Takougang E.M. (2009): Vibroseis survey acquisition in the central Nechako Basin, south-central British Columbia; *in* Geoscience BC Summary of Activities 2008, Geoscience BC, Report 2009-1, p. 145–150, URL <http://www.geosciencebc.com/i/pdf/SummaryofActivities2008/SoA2008-Calvert_original.pdf> [November 2011].

Dohaney, J., Andrews, G.D.M., Russell, J.K. and Anderson, R.G. (2010): Distribution of the Chilcotin Group, Taseko Lakes and Bonaparte Lake map areas, British Columbia; Geological Survey of Canada, Open File 6344, URL <http://geopub.nrcan.gc.ca/moreinfo_e.php?id=261655> [November 2011].

Ferri, F. and Riddell, J. (2006): The Nechako Basin project: new insights from the southern Nechako Basin; *in* Summary of Activities 2006, BC Ministry of Energy and Mines, pages 89–124, URL <http://www.em.gov.bc.ca/subwebs/oilandgas/pub/reports.htm> [November 2011].

Hannigan, P., Lee, P.J., Osadetz, K.G., Dietrich, J.R. and Olsen-Heise, K. (1994): Oil and gas resource potential of the Nechako-Chilcotin area of British Columbia; BC Ministry of Energy and Mines, Geofile 2001-6, 38 p. plus appendices and maps, URL http://www.empr.gov.bc.ca/Mining/Geoscience/PublicationsCatalogue/GeoFiles/Pages/2001-6.aspx [November 2011].

Hayes, B.J. (2002): Petroleum exploration potential of the Nechako Basin, British Columbia; BC Ministry of Energy and Mines, Petroleum Geology Special Paper 2002-3.

Hayward, N. and Calvert, A.J. (2009): Eocene and Neogene volcanic rocks in the southeastern Nechako Basin, British Columbia: interpretation of the Canadian Hunter seismic reflection surveys using first-arrival tomography; Canadian Journal of Earth Sciences, v. 46, p. 707–720.

Hayward, N. and Calvert, A.J. (2011): Interpretation of structures in the southeastern Nechako Basin, British Columbia, from seismic reflection, well log, and potential field data; Canadian Journal of Earth Sciences, v. 48, p. 1000–1020.

Idowu, O.A., Frederiksen, A.W. and Cassidy, J.F. (2011): Imaging the Nechako Basin, British Columbia, using ambient seismic noise; Canadian Journal of Earth Sciences, v. 48, p. 1038–1049.

Katsube, T.J. (2001): An analytical procedure for determining spectral induced polarization characteristics of anisotropic rocks, Yellowknife mining district, Northwest Territories; Geological Survey of Canada, Current Research 2001-E3, 29 p., URL <http://geopub.nrcan.gc.ca/moreinfo_e.php?id=212683> [November 2011].

Kim, H-S. (2010): Mapping crustal structure of the Nechako Basin using teleseismic receiver functions; M.Sc. thesis, University of Victoria, Victoria, BC, 112 p.

MacLaurin, C.I., Mahoney, J.B., James W. Haggart, J.W., Goodin, J.R. and Mustard, P.S. (2011): The Jackass Mountain Group of south-central British Columbia: depositional setting and evolution of an Early Cretaceous deltaic complex; Canadian Journal of Earth Sciences, v. 48, p. 930–951, doi:10.1139/e11-035

Mihalynuk, M.G., Orovan, E.A., Larocque, J.P., Friedman, R.M. and Bachiu, T. (2009): Geology, geochronology and mineralization of the Chilanko Forks to southern Clusko River area, west-central British Columbia (NTS 093C/01, 08, 09S); *in* Geological Fieldwork 2008, BC Ministry of Energy and Mines, Paper 2009-1, p. 81–100, URL <http://www.empr.gov.bc.ca/Mining/Geoscience/PublicationsCatalogue/Fieldwork/Documents/08_Mihalynuk_2008.pdf> [November 2011].

Mira Geoscience (2008): Development and application of a rock property database for British Columbia; Geoscience BC, Report 2008-9, 66 p., URL <http://www.geoscience bc.com/s/2008-09.asp> [November 2011].

O'Connell, R.J. and Budiansky, B. (1974): Seismic velocities in dry and saturated cracked solids; Journal of Geophysical Research, v. 79, p. 5412–5426.

Parsons, S., McGaughey, J., Mitchinson, D., Phillips, N. and Lane, T.E. (2009): Development and application of a rock property database for British Columbia; *in* Geoscience BC Summary of Activities 2008, Geoscience BC, Report 2009-1, p. 137–144, URL <http://www.geosciencebc.com/i/pdf/SummaryofActivities2008/SoA2008-Parsons_original.pdf> [November 2011].

Riddell, J.M. (2006): Geology of the southern Nechako Basin; BC Ministry of Energy and Mines, Oil and Gas Division, Petroleum Geology Map 2006-1, scale 1:400 000.

Riddell, J.M. (2011): Lithostratigraphic and tectonic framework of Jurassic and Cretaceous Intermontane sedimentary basins of south-central British Columbia; Canadian Journal of Earth Sciences, v. 48, no. 6, p. 870–896, doi:10.1139/e11-034

Salisbury, M. and Iuliucci, R. (2011): Physical rock properties database; Geological Survey of Canada–Atlantic, URL <http://gdr.nrcan.gc.ca/rockprop/rock_e.php> [November 2011].

Spratt, J. and Craven, J. (2011): Near-surface and crustal-scale images of the Nechako basin, British Columbia, Canada, from magnetotelluric investigations; Canadian Journal of Earth Sciences, v. 48, p. 987–999.

Sumner, J.S. (1976): Principles of Induced Polarization for Geophysical Exploration; Elsevier Scientific Publishing Company, Amsterdam., The Netherlands, 277 p.

Telford, W.M., Geldart, L.P., Sheriff, R.E. and Keys, D.A. (1976): Applied Geophysics; Cambridge University Press, London, United Kingdom, 860 p.

Walsh, J.B. (1965): The effect of cracks on the compressibility of rock; Journal of Geophysical Research, v. 70, p. 381–389.